ANL/--83-10

DE83 011931

Distribution Category:
Energy Conservation--
Industry (UC-95f)

ANL-83-10

ARGONNE NATIONAL LABORATORY
9700 South Cass Avenue
Argonne, Illinois 60439

TUBE VIBRATION IN INDUSTRIAL-SIZE TEST HEAT EXCHANGER (90° SQUARE LAYOUT)

by

H. Halle and M. W. Wambsganss

Components Technology Division

February 1983

DISCLAIMER

TABLE OF CONTENTS

LIST OF FIGURES

LIST OF TABLES

NOMENCLATURE

Symbol	Description
D	Tube diameter
f	Vibration frequency
m_{act}	Mass per unit length of tube
m_v	Virtual mass per unit length of tube
P	Tube pitch
Q	Flowrate
U	Mean crossflow velocity through minimum gap
$\bar{U}$	Reduced crossflow velocity, $\bar{U} = U/fD$, based on experimental frequency
U_r	Reduced velocity, based on theoretical frequency
U_{CR}	Reduced critical velocity, based on theoretical frequency
α	Exponential variation of pressure drop with flowrate
$\alpha_1, \alpha_2, \beta_1, \beta_2, \beta_3$	Empirical constants
γ	Pressure drop constant
Δp	Pressure drop, overall, inlet-to-outlet
δ_m	Mass damping parameter
ζ	Equivalent viscous damping ratio
ρ	Fluid density

Subscripts

cr	Critical, based on experimental data, at lowest flowrate initiating instability

Configuration Code

6 or 8	Number of crosspasses
10, 12, or 14	Nominal nozzle size
30 or 90	30° triangular or 90° square layout tube pattern
N	No-tubes-in-window bundle (otherwise full bundle)
F	Finned tubes (otherwise plain tubes)
X	Field or design fix

TUBE VIBRATION IN INDUSTRIAL SIZE TEST HEAT EXCHANGER (90° SQUARE LAYOUT)

by H. Halle and M. W. Wambsganss

ABSTRACT

Tube vibrations in heat exchangers are being systematically investigated in a series of tests performed with an industrial-size test exchanger. Results from waterflow tests of eleven different tube bundles, in six- and eight-crosspass configurations on a 90° square layout with a pitch-to-diameter ratio of 1.25 are reported. The test cases include full tube bundles, no-tubes-in-window bundles, finned tube bundles, and proposed field and design fixes. The testing focused on identification of the lowest critical flowrate to initiate fluidelastic instability (large-amplitude tube motion) and the location within the bundle of the tubes which first experience instability. The test results are tabulated to permit comparison with results obtained from previous tests with a 30° triangular layout tube bundle. Instability criteria are evaluated preliminarily. Pressure drop data are also generated and reported.

I. INTRODUCTION

Tube vibrations in industrial-sized shell-and-tube heat exchanger configurations are systematically investigated by means of a series of tests designed to obtain data under controlled conditions. These tests are part of an ongoing Heat Exchanger Tube Vibration Program which has the objective to contribute to the cost-effective design of industrial shell-and-tube heat exchangers capable of operating without flow-induced vibration damage. Besides the tests, the program includes the establishment of a data bank of collected tube vibration field experiences and the utilization of the data to contribute to improved current predictive methods and design criteria. The Heat Exchanger Tube Vibration Program is sponsored by the U.S. Department of Energy (DOE), Office of Energy Systems Research, under the Energy Conversion and Utilization Technology (ECUT) Program.

The tests experimentally investigate the effect of shellside water flow on the dynamic behavior of the tube bundle. Tubes in a heat exchanger will vibrate at virtually all flowrates to which they are exposed. At low flowrates the response is of low amplitude and typically random in character; a number of the closely spaced coupled modes are excited by turbulent buffeting of the flow. These vibrations are generally acceptable; however, consideration must be given to the potential for long term wear at the tube/support interfaces. When the shellside flowrate is increased to exceed

a threshold value, fluidelastic instability occurs. This is an excitation mechanism responsible for large amplitude vibration which, among other things, can result in tube-to-tube impacting and cause rapid tube failure. As such, it is the mechanism of most concern to designers and is the focus for this testing program.

A test exchanger, representative of a segmentally baffled, industrial-size, shell-and-tube heat exchanger has been designed and fabricated specifically for this test program. The exchanger is shown in Fig. 1 as installed in the Argonne National Laboratory's Flow Induced Vibration Test Facility (FIVTF), and is described in a later section of this report. The initial test work with tube bundles on a 30° triangular layout - oriented with one side of the equilateral triangle perpendicular to the flow direction - and with a pitch-to-diameter ratio of 1.25 has been reported previously [1,2]. The first test report [1] covers five different test cases of eight-crosspass (seven equally spaced baffles) bundles with different inlet/outlet nozzle diameters for bo full bundle and no-tubes-in-window (NTIW) configurations. A following report [2] presents the results of tests with six-crosspass (five equally spaced baffles) bundles, also on a 30° triangular layout with a 1.25 pitch-to-diameter ratio. The ten reported test cases include a full tube bundle, NTIW bundle, several proposed field fixes, and a bundle with finned tubes.

This report presents the results of eleven different test cases having a 90° square tube layout with a pitch-to-diameter ratio of 1.25. The test cases included various combinations of nozzle sizes, eight- and six-crosspass configurations, and full and NTIW bundles; in addition field and design fixes and finned tubes were tested with a 6-crosspass configuration.

The primary objective of the testing is to determine the critical flowrate for the initiation fluidelastic instability and to identify the location of the affected tubes within the bundle. Typically, the results indicate that tubes in the first row(s) past the baffle edge in the far window region, opposite the inlet/outlet nozzles, are the first to experience instability. As the flow is increased further, adjacent groups of tubes in the far window region participate in the instability. Further increase of the flowrate may initiate instability in the near window region, adjacent to the nozzles. Generally, hysteresis is observed in the sense that the flowrate at which instability ceases is below the threshold level for the onset of instability. This implies that fluid transients may trigger instability at flowrates below the critical flowrate encountered with increasing flow. Comparisons show that the 90° square layout bundles experienced instability at a lower critical flowrate than 30° triangular layout bundles having an otherwise corresponding configuration. The tests

of field and design fixes indicate that the onset of instability can be delayed to a higher critical flowrate.

In addition, pressure drop measurements were taken to contribute to the understanding of heat exchanger performance.

It should be noted that Heat Transfer Research, Inc. (HTRI), a not-for-profit research organization with over 175 members representing heat exchanger designers, manufacturers, and users, is retained as a consultant to the program. HTRI serves as an important two-way link with industry, it provides the needed input relative to practical commercial designs, problems experienced in the field, field and design fixes, and assists to transfer the results of this test program to the industry.

II. BACKGROUND

The second of the subject program's test reports [2] presented an extensive discussion of the background information, divided into the main topics of "instability mechanisms" and "criteria for determining critical flow." The latter lists five criteria: sensory observations, vibration amplitude vs. flow-response rate, vibration amplitude vs. flow-amplitude threshold, flow sweep-time history, and frequency response data. As discussed in Ref. 2, each of the five criteria has advantages and disadvantages relative to another. In the analysis and interpretation of data from the subject tests, all five methods are employed to various degrees. However, a heavier reliance is placed on time histories from flow sweeps and examination of the rate of increase of vibration response with flowrate (vibration amplitude vs. flow-response rate criterion) to identify the abrupt increase in response which characterizes the onset of instability. The reader is referred to the detailed presentation in the "background" chapter of Reference 2.

III. TEST DESCRIPTION

A. Test Exchanger and Flow Facility

The test exchanger is a segmentally baffled shell and tube exchanger, representative of an industrial heat exchanger. It is specially designed to permit easy assembly/disassembly necessary to provide different tube bundle configurations. There is no flow on the tubeside, the tube ends are open to readily permit observation or instrumentation. The exchanger is piped to Argonne's Flow-Induced Vibration Test Facility (FIVTF) as shown in Fig. 1. The FIVTF has four pumps which can be operated in combinations to deliver a maximum water flowrate of up to 0.50 m^3/s (8,000 gpm) to the shellside of the bundle. Figure 2 shows the tube bundle on a specially built transporter

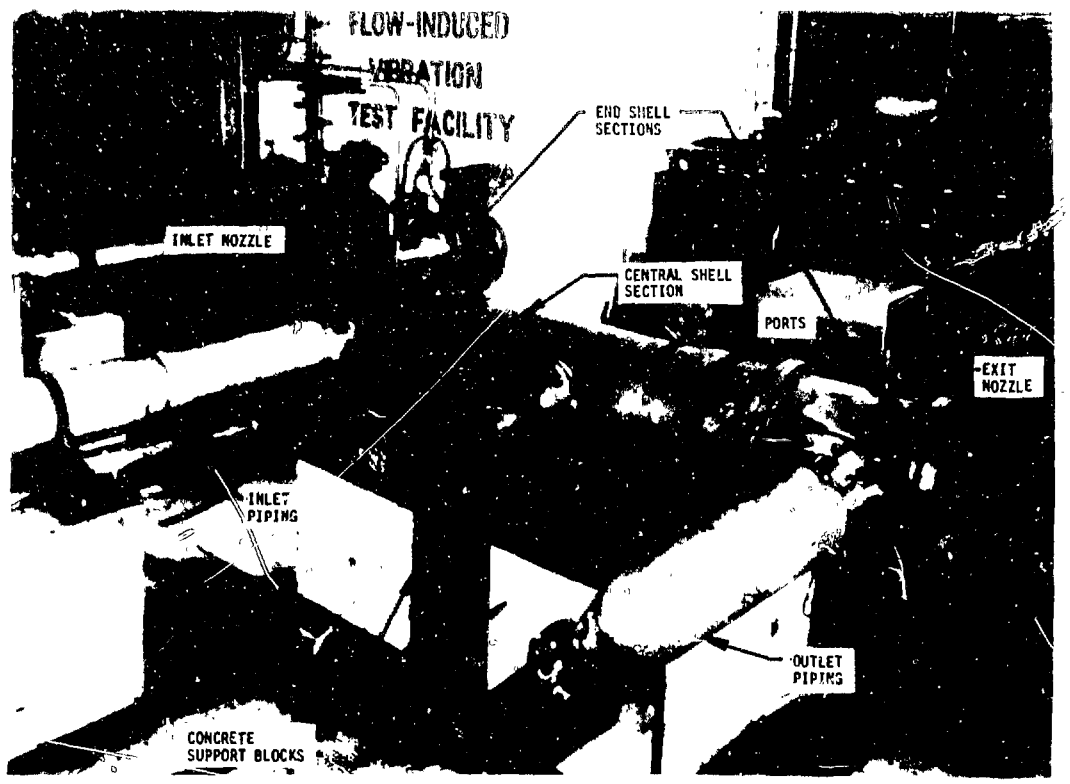

Fig. 1. Test exchanger installed in Flow-Induced Vibration Test Facility (FIVTF). ANL Neg. No. 113-79-100A.

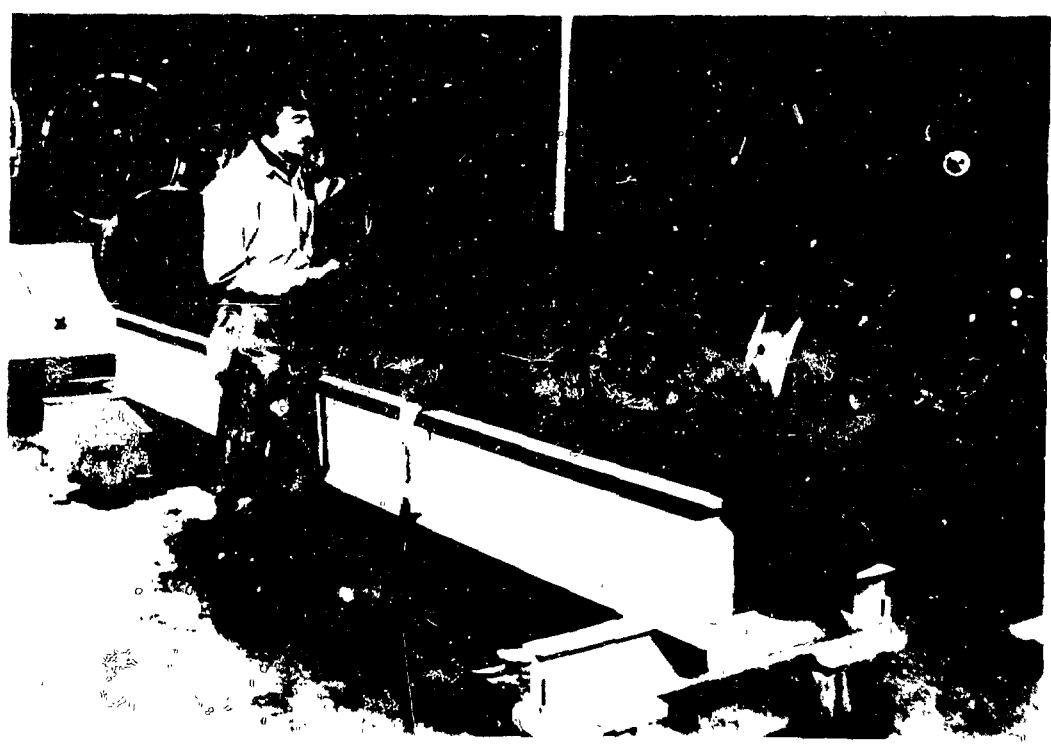

Fig. 2. Test exchanger in eight-crosspass, full tube bundle configuration. ANL Neg. No. 113-81-43.

prior to insertion into the shell seen in the left background. A spare baffle plate is also displayed.

The general features, dimensions, and data of the test exchanger are given on Tables 1 and 2. To facilitate comparison of the 90° square layout with the earlier 30° triangular layout tests, all pertinent data are included.

The heat exchanger is configured with eight or six crosspasses, having seven or five equally spaced baffles, as shown on Figs. 3 and 4 schematically. Figure 5 shows the 90° square layout pattern and the system adopted to identify tube location. For the eight-crosspass configuration shown, the baffle cut is 25.5 percent of the shell inside diameter providing saddle-type support at alternate baffles for tubes in rows F and R. For the six-crosspass configurations the baffle cut was increased by a tube row to 29.6 percent, providing saddle support for the tubes of rows G and Q.

To provide a perspective value for the flow regimes, an estimate of the Reynolds' number for the full tube bundle has been computed based on the available flow area in the central plane of the test exchanger normal to the flow, assuming no leakage, and using the tube diameter as the characteristic dimension. On that simplified basis the Reynolds' numbers at the 0.126 m^3/s (2000 gal/min) flowrate for the 30° triangular tube layout pattern are approximately 42,000 and 31,000 for the 8- and 6-crosspass configurations, respectively; for the 90° square pattern the corresponding values are 36,000 and 27,000.

For the eight- and six-crosspass configurations, the maximum unsupported tube lengths of the plain test exchanger tubes are respectively 68 and 90 percent, i.e., within the limit, of the maximum length recommended by the TEMA standards [3] used by many industries. The maximum unsupported length of the finned tubes in the six-crosspass configuration, however, exceeds the TEMA standards by about 16 percent.

B. Test Cases

Eleven different configurations, all having a 90° square tube layout pattern, were tested as part of this test series. The test cases, defined by case numbers 16-26, are summarized in Table 3 and briefly discussed below. Test cases 16 and 17 as well as 19 and 20 comprise two pairs of test cases that would permit evaluation of the effect of inlet/outlet nozzle size on full tube bundle instability for the eight and six crosspass arrangements, respectively. Cases 18 and 23 (Fig. 6a and c) represent no-tubes-in-window (NTIW) configurations. Heat exchanger designers resort to this somewhat drastic step of foregoing heat transfer capacity in the window regions to ensure against a vibration problem. The reduced pressure drop of NTIW tube bundles may help to somewhat alleviate the heat transfer performance

Table 1. General features and basic dimensions of test exchanger

Shellside fluid	Water
Tubeside	No fluid, open tubes, ready insertion of instrumentation
Shell (Stainless steel), I.D.	0.59 m (23.25 in.)
Shell, inside length (tubesheet spacing)	3.58 m (140.75 in.)
Modular shell construction	Flexibility to change nozzle orientation
Nozzles, inlet and outlet	Insertion of piping to reduce inside diameter permits providing three nominal sizes/inside diameters 14-in. size/337 mm (13.25 in.) I.D. 12-in. size/288 mm (11.328 in.) I.D. 10-in. size/241 mm (9.500 in.) I.D.
Nozzles at shell midspan	Observation ports or alternate flow route (e.g., direct crossflow)
Tube bundle	Removable unit, ready assembly/ disassembly
Tubesheets	One stationary, one floating; special double tubesheet construction to contain O-rings to seal tubes
Tie bolts	Stainless steel rods in tube locations Secure and space tubesheets on both ends of heat exchanger Compress double tubesheets on each end to seal O-rings Same O.D. as tubes
Tie bars	Secure and space baffle plates, smaller O.D. than tubes

Table 2. Tube and tube bundle data

Tube, plain (Admiralty brass)	
O.D.	19.1 mm (0.750 in.)
Wall thickness	1.2 mm (0.049 in.)
Tube, finned (Admiralty brass), 19 fins/in.	
O.D.	19.1 mm (0.750 in.)
I.D., unfinned plain tube at end or land	15.7 mm (0.620 in.)
Root diameter, finned section	15.9 mm (0.625 in.)
I.D., finned sections	13.8 mm (0.541 in.)
Equivalent "squashed" diameter, finned section	16.9 mm (0.666 in.) est.
Tube layout patterns	
30° triangular	One side of equilateral triangle normal to flow
90° square	Sides parallel and normal to flow
Pitch-to-diameter ratio	1.25
Number of crosspasses	8 (i.e., 7 baffles) 6 (i.e., 5 baffles)
Number of tubes (not counting 11 tie bolts and 8 tie bars)	
30° triangular layout	488, full tube bundle 326, NTIW, 8 crosspass 286, NTIW, 6 crosspass
90° square layout	410, full tube bundle 276, NTIW, 8 crosspass 238, NTIW, 6 crosspass
Baffle spacing	448 mm (17.6 in.) approx., 8 crosspass 597 mm (23.5 in.) approx., 6 crosspass
Baffle (brass) thickness	9.5 mm (0.375 in.)
Tube/Baffle hole clearance	0.4 mm (0.016 in.) minimum
Cut of single segmental baffles	
30° triangular layout	25.5%, 8 crosspass 28.9%, 6 crosspass
90° square layout	25.5%, 8 crosspass 29.6%, 6 crosspass

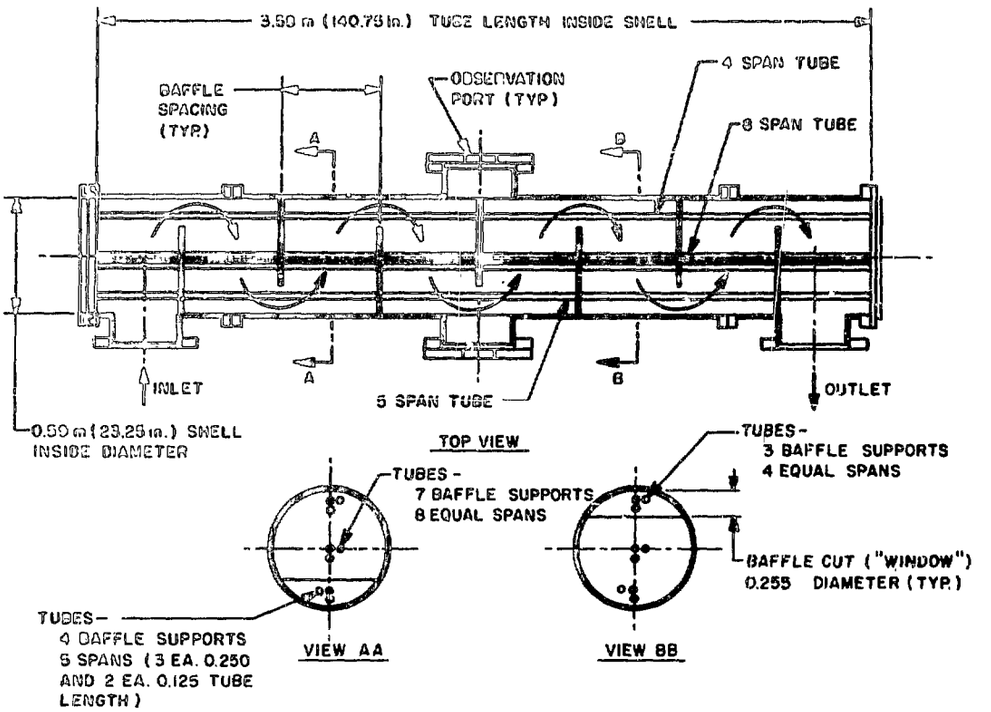

Fig. 3. Test exchanger, eight-crosspass configuration

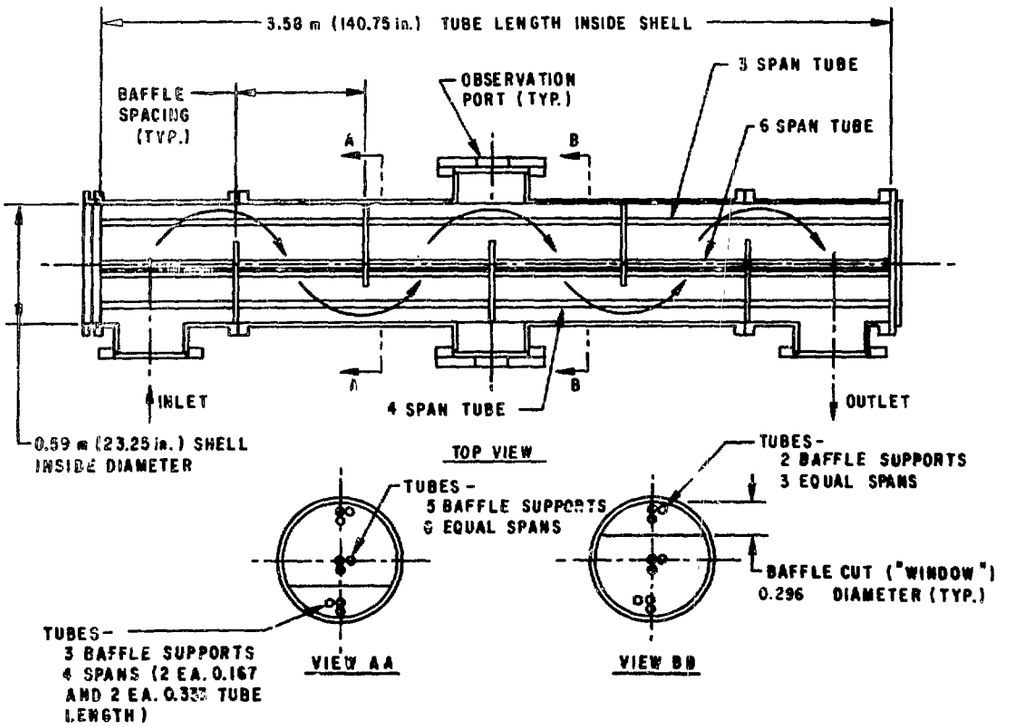

Fig. 4. Test exchanger, six-crosspass configuration

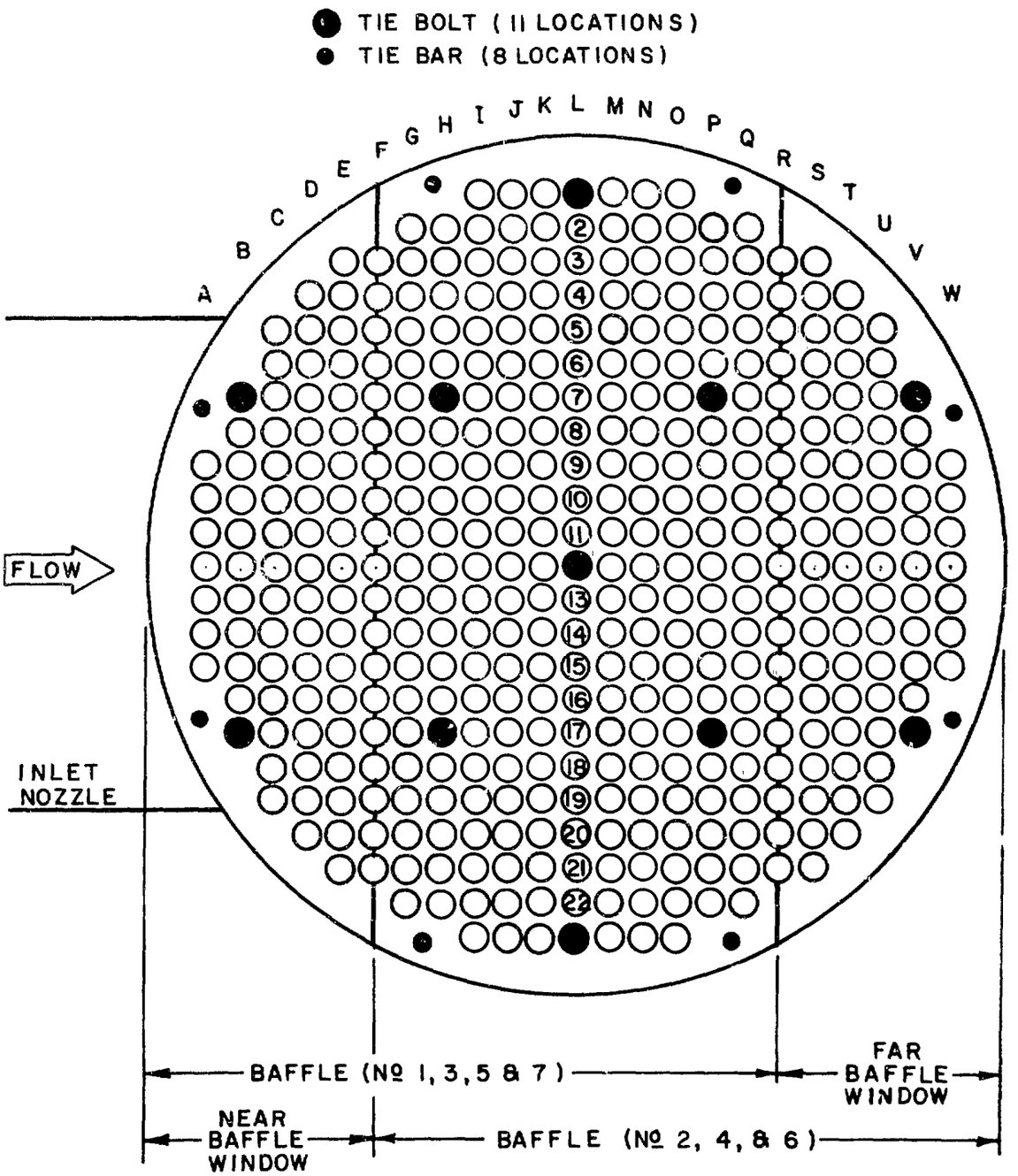

Fig. 5. Tube layout and identification

Table 3. 90° square layout test cases

Case No.	No. of Cross-passes	Nominal inlet/outlet nozzle size (in.)	Tube Bundle Configuration
16	8	10	Full bundle
17	8	14	Full bundle
18	8	14	NTIW bundle (Fig. 6a)
19	6	14	Full bundle
20	6	10	Full bundle
21	6	10	Field fix: pass lane in far window region (Fig. 6b)
22	6	10	Field fix: pass lane in both window regions (Fig. 6d)
23	6	10	NTIW bundle (Fig. 6c)
24	6	10	Design fix: FIVER; auxiliary baffles in flow turn-around regions
25	6	10	Full bundle; finned tubes
26	6	10	NTIW bundle; finned tubes (Fig. 6c)

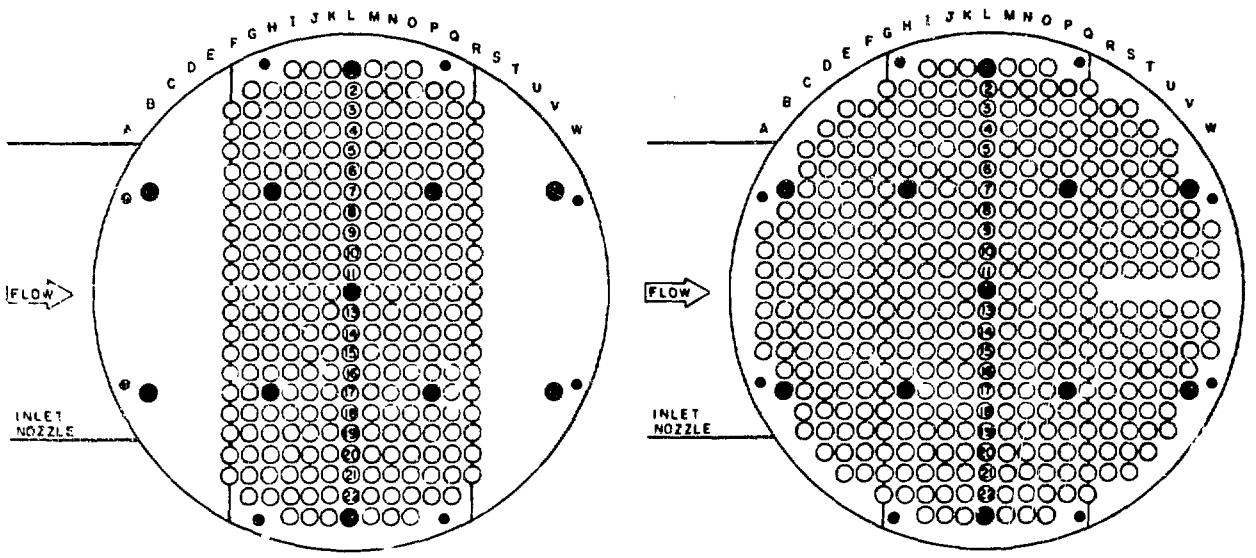

Fig. 6. Schematic representation of NTIW configurations anf field fixes: (a) Case 18, (b) Case 21, (c) Cases 23 and 26, (d) Case 22

characteristics. Cases 21 and 22 (Fig. 6b and d) investigate the effect of a pass lane in one or both windows, respectively. These comprise field fixes which may be utilized to increase the critical flow velocity, with possible penalty on heat transfer performance, of an exchanger installed in the field. Case 24 (Figs. 21-22) provides a design fix called the Flow-Induced Vibration Evasion Restraint (FIVER) concept, which features auxiliary baffles and significantly increased the critical flow velocity. Finally, the performance of finned tubes was tested with a full bundle, case 25, and a NTIW configuration, case 26 (Fig. 6c).

C. Test Procedure/Data Processing

For the sake of completeness some of the discussion presented on this topic in the previous test reports [1,2] is repeated here. It is practically not possible to instrument all of the more than 400 tubes in the bundle, or even the somewhat smaller number of tubes in the window regions that will be more susceptible to vibration by virtue of their lower natural frequencies. To gain insight to the overall dynamic behavior of a particular tube bundle, the initial flow test is typically performed without the tubes instrumented. The flow is increased in step changes and the tube bundle backlit to facilitate the visual detection of tube motion by sighting down the tube bores; large amplitude tube motion associated with instability is readily detected with this technique. The onset of instability can also be determined from the sudden increase in audible noise coming from the unit. From visual observation of the overall bundle response, the tubes first experiencing large amplitude vibration are identified. It is from this group that tubes are selected to be instrumented.

The 90° square layout permitted observation all-the-way-through the horizontal gaps in the central region of the tube bundle visible through the observation ports. Thus the tube bundle could be backlit in this manner also. Observation of the vibrating tubes, using stroboscopic light at times, was interesting, but not as scientifically informative as had been hoped.

Subsequent water flow tests are performed with selected tubes instrumented with miniature accelerometers. The accelerometers are mounted on specially designed plugs and are inserted into the tubes. Usually the accelerometers are located at the axial location expected to have the largest amplitude of the vibration mode corresponding to the frequency that is being measured. Experience indicated that with few exceptions, to be discussed in later sections, the tubes vibrated at the lowest natural frequency corresponding to the first bending mode. Accordingly, the accelerometers in the far window tubes were located at about 55 percent of the spanlength from the inlet tube sheet, i.e., just slightly beyond the

baffle location in the first flow turnaround region. The accelerometers for the near window tubes were usually located midspan of the first long span, i.e., opposite the baffle in the second turnaround. These locations are also suitable to sense second bending mode vibration amplitudes, if indeed they occur. In almost all cases the accelerometers are oriented to be sensitive in the vertical, which is the lift, i.e., transverse-to-flow, direction. This was done because it appears that tubes usually initiate impacting upon instability by large out-of-phase vibration in that direction. However, a biaxial set-up was used for one of the most susceptible tubes. In addition, at least one accelerometer was mounted externally on the shell of the test exchanger to monitor its vibration response. This was considered of practical importance, since the outside of the shell may be the only location that is readily accessible for an existing heat exchanger. However, no significant conclusions have been obtained from the investigations of the recorded signals performed to date.

The flowrate is increased in steps and at each step the acceleration-time signals are recorded on FM magnetic tape. In some tests, slow "flowrate scans" are employed. In these cases both the changing flowrate and the corresponding acceleration signals are simultaneously recorded as a function of time.

The data processing of the tape recorded signals generated by the tube-mounted (and one or two shell-mounted) accelerometers makes extensive use of a sophisticated Fast Fourier Transform Analyzer. This is essentially a specialized mini-computer supplemented by a graphics package to allow the preparation of hard copies. The signals from the constant flowrate runs are used to obtain and plot accelerometer and (by double integration) displacement power spectral density curves and the corresponding integrals. This is a fairly routine task - but these must then be examined by experienced personnel to determine principal frequencies and root-mean-square (rms) amplitudes. The signals from the "flowrate scans" were utilized to pinpoint the flowrate at the instant of instability initiation or cessation. This is not a routine task, because the thresholds have to be "caught" at the proper instant from the tape. Recorded time code signals greatly facilitate this job.

In addition to the acceleration signals, pressures are measured at the shell inlet and outlet and at various intermediate locations on the shell wall after each incremental increase in flowrate.

IV. FLOW TESTS: TUBE BUNDLE VIBRATION

This chapter deals specifically with the performance of flow tests to obtain tube bundle vibration information for the 90° square layout configurations of test cases 16 through 26. Chapter V presents an overview of all

tests performed to date under this program. This overview includes a test matrix that indicates how any particular test fits into the overall scheme.

The flow tests were performed following the test procedure outlined in Section III.C. The threshold flowrate was usually determined by the initiation of impacting. Sensory (sight, sound, feel) observations are documented in the Appendix for each of the test cases. Based on these observations, the lowest critical flowrate for a given bundle configuration (test case), and the flowrate at which instability ceases, as flowrate is decreased, are determined. These results are summarized in Tables 4 and 5 for all except the NTIW test cases.

Case 16

Case 16 is a 8-crosspass, 7-baffle full tube bundle configuration with 10 in. size inlet/outlet nozzles. The baffle cut is 25.5 percent (of the inside shell diameter) locating the baffle edge for this and the following 8-crosspass tests near the center of rows F and R. Flowrates up to 0.226 m^3/s (3580 gal/min) were applied. The flowrate-dependent tube vibration response differed in various regions (Table 4) of the test exchanger as described below.

Fluidelastic instability initiated in the central region of tube row S next to the baffle edge in the "far" window opposite of the inlet and outlet nozzles, at 0.148 m^3/s (2340 gal/min), when amplitudes, determined from time histories from a flow sweep, increased significantly within 10 to 20 cycles to result in impacting with adjacent tubes. The threshold is indicated by the sharp amplitude rise of tube S-12V (V for vertical, transverse-to-flow, orientation of this biaxially instrumented tube) as shown on Fig. 7. The principal vibration frequencies, obtained from frequency spectra analysis, are shown on Fig. 8. The spectra (Fig. 9) indicate the broad band response due to buffeting, and the multiple frequency, low amplitude response prior to instability; the sharp tuning at and near instability; and a double two-frequency beating above the instability threshold. Generally the vibration amplitudes were not constant but indicated beating and thus periodic impacting at roughly 2 Hz. As the flowrate was increased beyond the instability threshold, additional groups of tubes were successively excited: when 0.202 m^3/s (3200 gal/min) was reached, almost all the tubes in the far window had been excited into significant vibrations. There was little hysteresis because with decreasing flow the instability ceased at about 0.144 m^3/s (2280 gal/min). Except for the flowrates near the critical, the frequency response was fairly broadband and noisy: prior to instability due to turbulent buffeting; afterwards due to impacting.

The vibration response of the bottom tubes (near the shell periphery) in the rows near the baffle cut in the "far" window was somewhat different

than that of the central tubes (Figs. 10-12). Here the vibration amplitudes increased gradually with increasing flowrates. In the case of the instrumented bottom tube S-21 next to the baffle edge, the amplitudes became sufficiently large to result in impacting (presumably with its upper neighbor) at about 0.144 m^3/s (2280 gal/min), as determined from time histories from a flow sweep. Much larger flowrates (estimated to be about 0.189 m^3/s (3000 gal/min)) were required to vibrate the top tubes (of row S and its neighbors) in a corresponding manner. The difference in behavior can probably be explained by the eccentric position of the tube bundle resting on the bottom of the shell. This results in unsymmetric top versus bottom flow distributions. This is caused by baffle-to-shell clearances that are very much larger on top than on the bottom of the bundle, where they approach zero in the center. The tube bundle to shell clearance is similarly, though not as drastically, affected. These differences of the tube response were not observed as distinctly when the triangular tube bundles were tested.

This type of dynamic response behavior, viz., a gradual increase to large amplitude motion, is not uncommon, especially with dense fluids, and has been observed in laboratory tests [4]. However, as discussed in an earlier report [2], it does make definition of a critical flowrate more difficult as there is no abrupt increase in response to positively identify the threshold. In such cases the criterion based on frequency response spectra is useful: instability is defined as the flowrate at which transition from a broad-band, multi-frequency spectrum to a well-defined, single-frequency spectrum occurs. In examining the frequency spectra of Fig. 12 one observes that a single frequency spectrum first occurs at a flowrate of 1800 gpm. This indicates that instability initiated prior to this flowrate.

The occurrence of the instability threshold for tube S-21 at a flowrate significantly less than that for the central tubes in row S can, in all likelihood, be attributed to the local flow conditions as described above. In addition, it is possible that the instability mechanism may be of a different type from that responsible for the large amplitude motion of the tubes in the central portion of the window region; Connors [5] discusses fluidelastic instability due to "skimming" flow which is similar to the situation with tube S-21.

In the "near" window, next to the nozzles, vibrations, often occurring at higher than fundamental frequencies, could be observed or felt with the fingertips at the tube ends at increased flowrates. Instability occurred in the central region of row E next to the baffle edge at 0.220 m^3/s (3480 gal/min); the acceleration signals of the instrumented tube E-12 indicated an instantaneous initiation of violent excursions without any - even brief - vibration buildup. The resulting collisions apparently affected this tube

Table 4. Flowrates associated with instability and tube impacting or with large vibration amplitudes at different locations in tube bundle. Cases 16, 17, 19, and 20

90° square tube layout, plain tubes, full bundles

Location/Phenomenon	Case 16 8-Crosspass Full bundle 10 in. nozzles m^3/s (gal/min)	Case 17 8-Crosspass Full bundle 14 in. nozzles m^3/s (gal/min)	Case 19 6-Crosspass Full bundle 14 in. nozzles m^3/s (gal/min)	Case 20 6-Crosspass Full bundle 10 in. nozzles m^3/s (gal/min)
Far window, central region				
Instability initiates	0.148 (2340)	0.149 (2360)	0.101 (1600)	0.104 (1650)
Instability ceases upon flow reduction	0.144 (2280)	0.149 (2360)	0.097 (1540)	0.091 (1440)
Far window, near shell periphery, at bottom (refer to text)				
Onset of instability based on frequency response data	0.114 (1800)			
Large vibration amplitudes are excited	0.144 (2280)*	0.124 (1960)**	0.137 (2170)	0.148 (2350)
Large amplitudes cease upon flow reduction	***	***	0.120 (1900)	0.115 (1830)
Near window, central region, near baffle edge				
Instability initiates	0.220 (3480)	0.223 (3530)	0.157 (2490)	0.151 (2400)
Instability ceases upon flow reduction	0.177 (2800)	0.168 (2660)	0.123 (1950)	0.109 (1720)

*Impacting

**Probable occasional impacting, may be overconservative as unacceptability criterion.

***Gradual amplitude vs. flowrate change

Table 5. Flowrates associated with instability and tube impacting or with large vibration amplitudes at different locations in tube bundle. Cases 21, 22, 24, and 25

90° square layout, 6 crosspasses, 10 in. nozzles

Location/Phenomenon	Case 21 Plain tubes Field fix One passlane m^3/s (gal/min)	Case 22 Plain tubes Field fix Two passlanes m^3/s (gal/min)	Case 24 Plain tubes Design fix FIVER m^3/s (gal/min)	Case 25 Finned tubes Full bundle m^3/s (gal/min)
Far window, central region				
Instability initiates	0.122 (1930)	0.132 (2100)	0.177 (2800)*	0.147 (2330)
Instability ceases upon flow reduction	0.109 (1720)	0.120 (1900)	0.167 (2640)	0.109 (1720)
Far window, near shell periphery, at bottom (refer to text)				
Large vibration amplitudes are excited	0.145 (2300)	0.175 (2770)		
Large amplitudes cease upon flow reduction	0.134 (2120)	0.119 (1880)		
Near window, central region, near baffle edge				
Instability initiates	0.175 (2780)	0.223 (3530)		0.188 (2980)**
Instability ceases upon flow reduction	0.174 (2760)	0.187 (2970)		0.154 (2440)**
Near window, first row A tubes				
Instability initiates				0.226 (3590)

*Unacceptable vibration performance - in near window region - encountered at lower flow rates, see text

**Probably overly conservative, data taken during fast transient flow reduction

Case 16

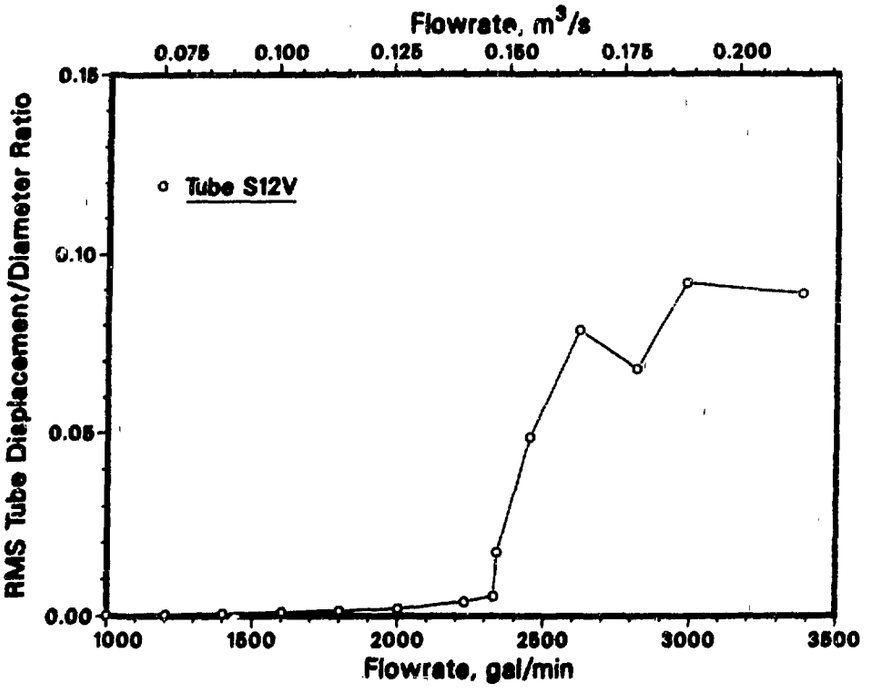

Fig. 7. RMS displacement versus flowrate: Case 16, tube S-12V

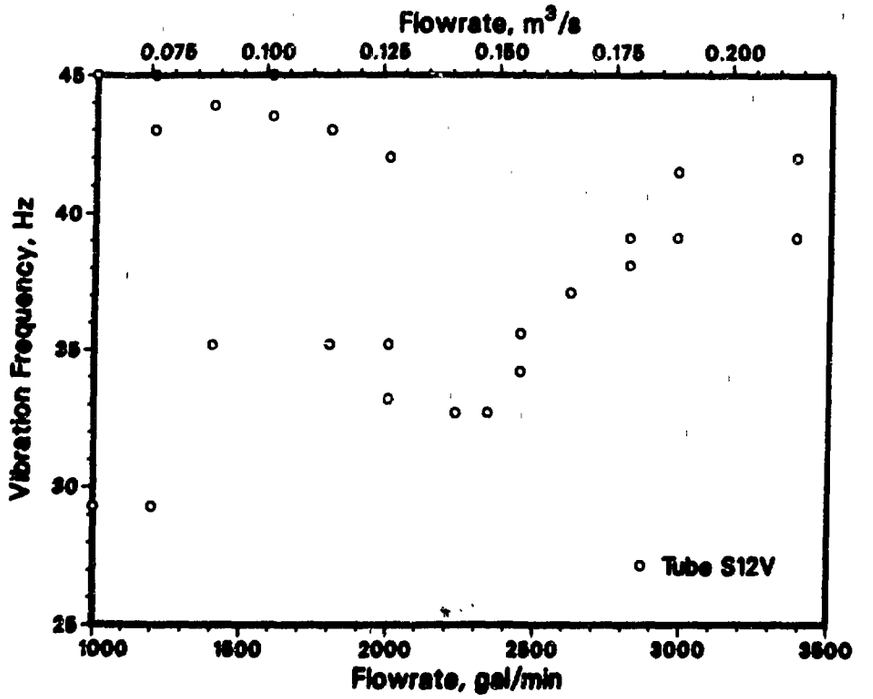

Fig. 8. Frequency versus flowrate: Case 16, tube S-12V

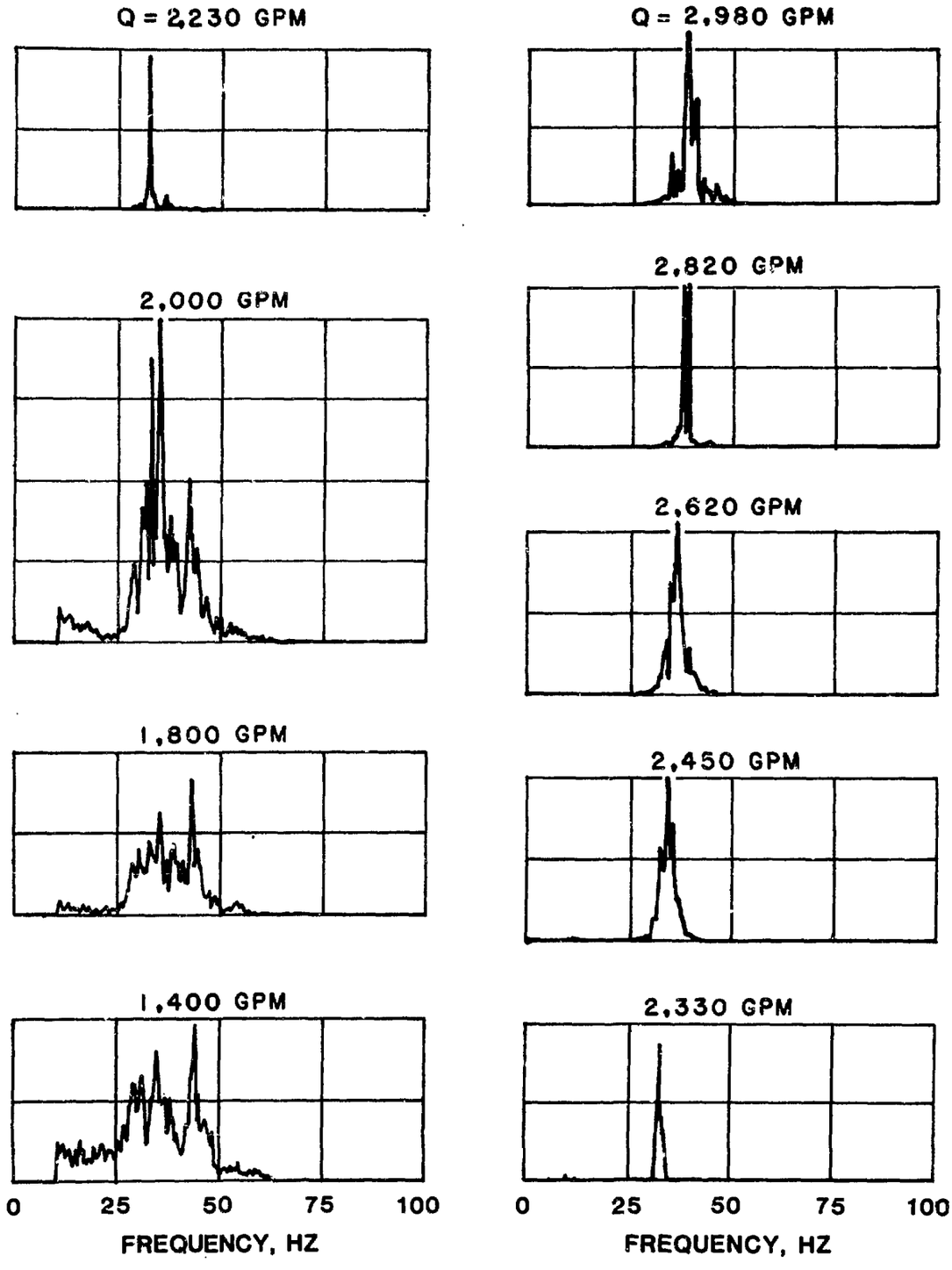

Fig. 9. Frequency response spectra: Case 16, tube S-12V

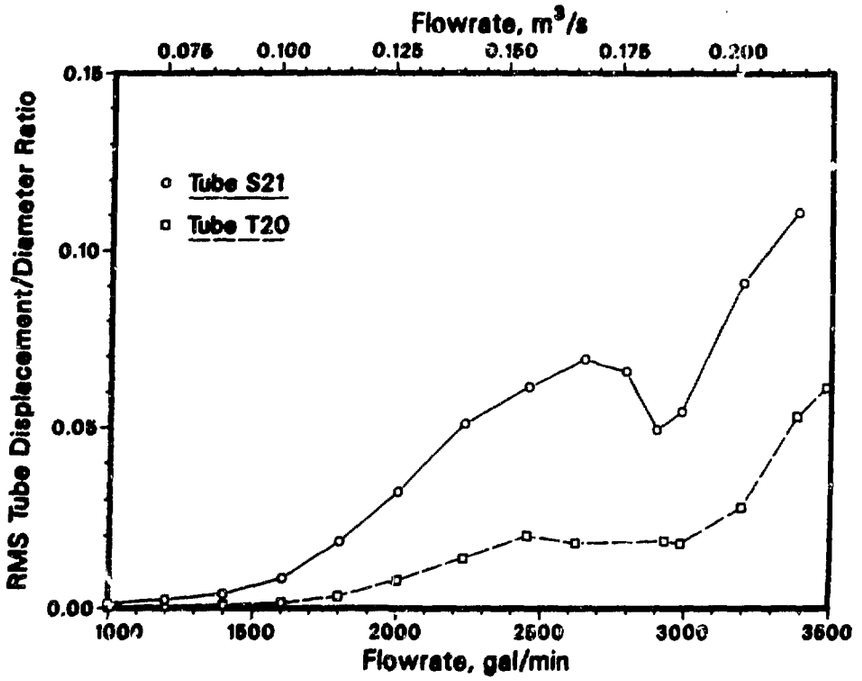

Fig. 10. RMS displacement versus flowrate: Case 16, tubes S-21 and T-20

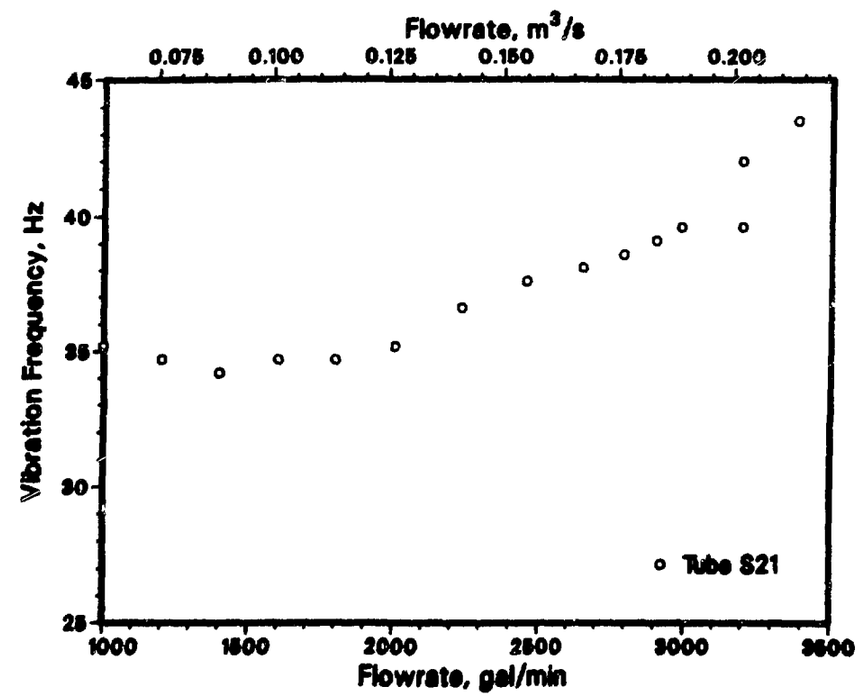

Fig. 11. Frequency versus flowrate: Case 16, tube S-21

Q=3,230 GPM

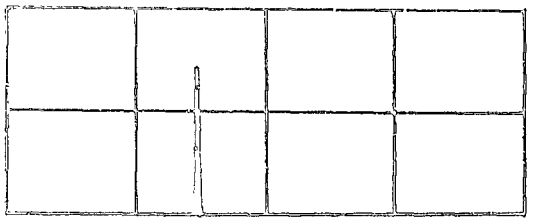

2,000 GPM

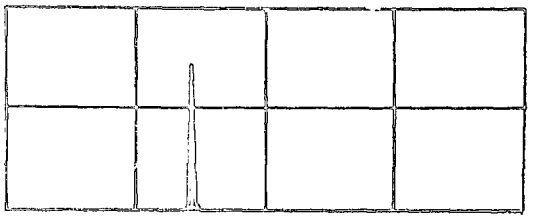

1,800 GPM

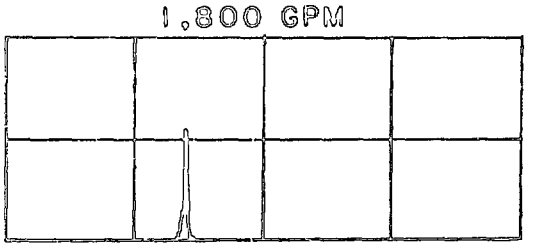

1,400 GPM

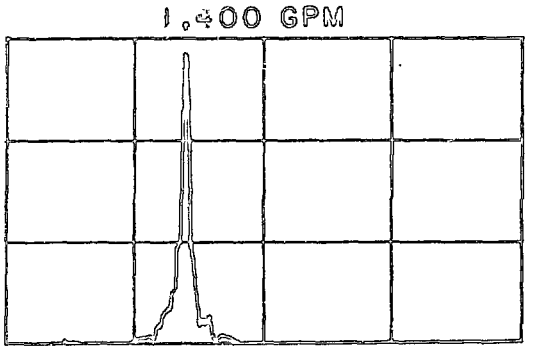

1,000 GPM

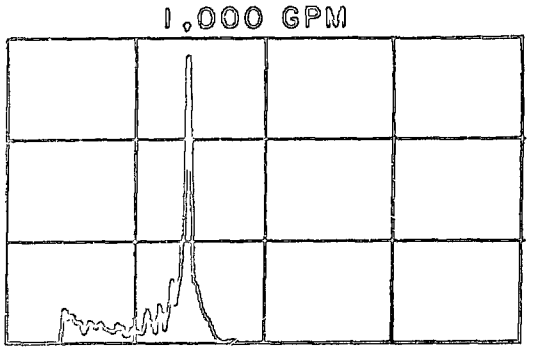

0 25 50 75 100

FREQUENCY, HZ

Q=3,380 GPM

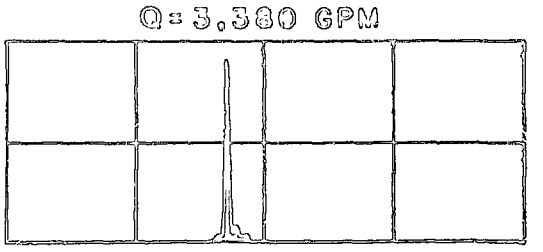

3,190 GPM

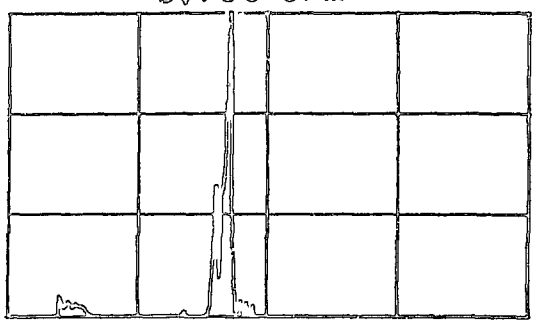

2,980 GPM

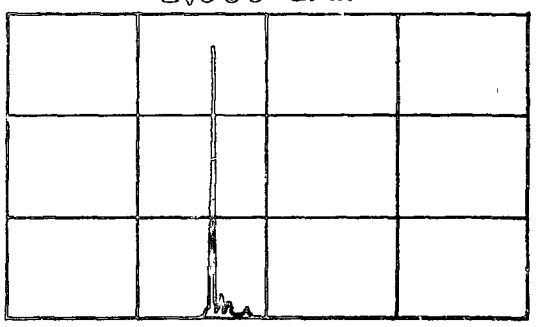

2,790 GPM

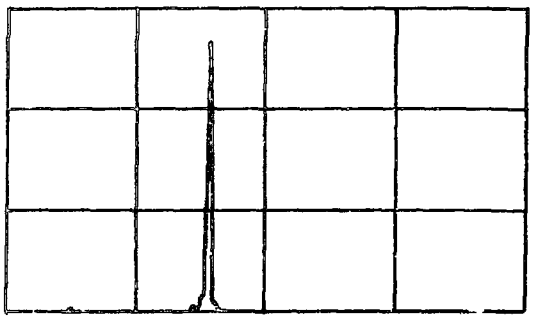

2,450 GPM

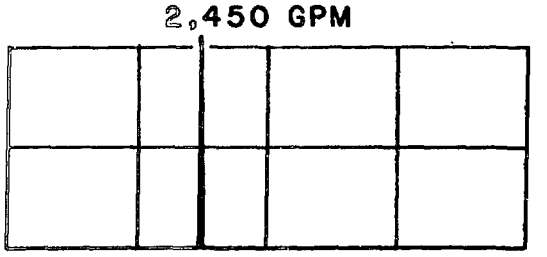

0 25 50 75 100

FREQUENCY, HZ

which, upon flow rate reduction, vibrated with a much more distinct frequency (about 35 Hz) and stopped impacting at about 0.177 m^3/s (2800 gal/min).

Case 17

Case 17 is an 8-crosspass, tube bundle configuration with 14 inch nominal size nozzles. The test results indicated a behavior quite similar to those obtained earlier during case 16 testing with the same tube bundle but 10 inch size nozzles. The principal test results compared on Table 4 indicate quite similar results; it is seen that the fluidelastic tube vibration instabilities in rows S and T began at only slightly higher flowrates for case 17 with the 14 inch nozzles. The data in Table 4 indicate the large difference of the instability threshold and of the amount of hysteresis observed when the responses of the tubes in the far window opposite the inlet/outlet nozzles and in the near window adjacent to the nozzles are compared. The case 16 discussion detailed the different flow-dependent tube vibration responses in different regions of the test exchanger. One phenomenon, that distinguished these 90° square layout, 8-crosspass, full tube bundle tests, is that there was at least one tube, the bottom tube (S-21) in the row next to the baffle edge in the far window, that, based on the frequency response spectra and magnitude of vibration amplitude, appears to have experienced instability at a lower flowrate than generally determined for the other tubes in the far window region. For reasons discussed below, it is difficult to determine at exactly what flowrate the tube vibration becomes unacceptable; however, it can be stated a flowrate of 0.144 m^3/s (2280 gal/min) is definitely unacceptable. Defining the threshold at 0.124 m^3/s (1960 gal/min) on Table 4 may be overly conservative because the occasional sharp spikes observed on the acceleration signal may be indicative of rattling against the baffle plates; however, sharp tube-to-tube or tube-to-baffle impact cannot be ruled out. Reasons that make the determination of a threshold flowrate difficult are the gradual rise of vibration amplitude with flowrate (there is no abrupt increase in vibration response typical of an instability) and the probability that the accelerometer was not mounted in the tube span having the largest vibration amplitude and containing the first impact location upon impact initiation. Factors that possibly contribute to the performance of the subject tube and its neighbors are the expected large leakage flows in the gap between the tube bundle and the internal shell surface and the flow orientation which at these locations probably encounters what is essentially a 45° rotated square rather than the nominal 90° pattern.

In preparation for the subsequent test with no-tubes-in-window configuration, all 4- and 5-span tubes in the window region were removed from the bundle. These tubes were examinned for tube-to-tube impact evidenced by midspan polish marks. With very few exceptions, these marks were on top

and/or bottom of the tubes, indicative of large vibration amplitudes in the transverse-to-(the plane of) flow direction. The few exceptions occurred on tubes near the shell periphery, where the flow direction can deviate substantially from the nominal 90° orientation. On the four-span tubes in the far window the impact marks were usually more prominent in the two central spans than in the spans adjacent to the tubesheets. When the incidence of tube impact marks is mapped on the tube layout pattern, the occurrence of impacting is sseen to be slightly biased towards the top of the test exchanger. The removed window tubes were also examined for wear marks caused by the baffle holes. In some regions of the test exchanger, these marks had fairly consistent orientations as shown on Fig. 13. Probably both time-constant as well as superimposed dynamic forces were at work. The significance of the resulting patterns has not been explored to date.

Case 18

Case 18 is an 8 crosspass (7-baffle) configuration with 14 inch size inlet/outlet nozzles and with all tubes in both window regions, rows A through E and S through W, removed to provide a no-tubes-in-window (NTIW) configuration (Fig. 6a). All tubes remaining in the bundle were supported by all baffles or at least alternately supported and saddled in the baffles. The window area of the baffles were fitted with sheet metal plates to cover the unused baffle holes. The unused tubesheet holes were plugged and sealed. Flowrates up to 0.303 m^3/s (4800 gal/min), well beyond industrial practice, were applied but no significant tube vibrations were observed. The NTIW bundle still contained the eight tie bars, which consist of 9.5 mm (0.375 in.) diameter rods with sections of 12.7 mm (0.5 in.) O.D. tube slipped over them that serve to space and secure the baffle plates. Thus the tie bars are smaller, and even though made of stainless steel, much more flexible than the test exchanger tubes. As a consequence of the removal of the surrounding tubes in the window region, four of these tie bars were exposed to the flow. These tie bars were subject to violent flow induced vibrations. The pressure differences in the test exchanger placed the tie bars into compression, thus reducing natural frequency and increasing susceptibility to vibration. At the maximum applied flowrate the pressure drop across the heat exchanger rose to about 340 kPa (50 $lb/in.^2$), very high compared to industrial practice, and upon the second exposure to this pressure drop several tie bars suddenly buckled and the tests were concluded.

Aside from relocation or stiffening of exposed tie bars, these tests illustrate the existence of two design options. The present arrangement of the test exchanger places the tie bars in compression but does not require the tie bars to extend into the inlet region of the test exchanger. On the other hand, the designer may have the choice of anchoring the tie bars to the inlet side tubesheet thus exposing them to direct inlet flow conditions

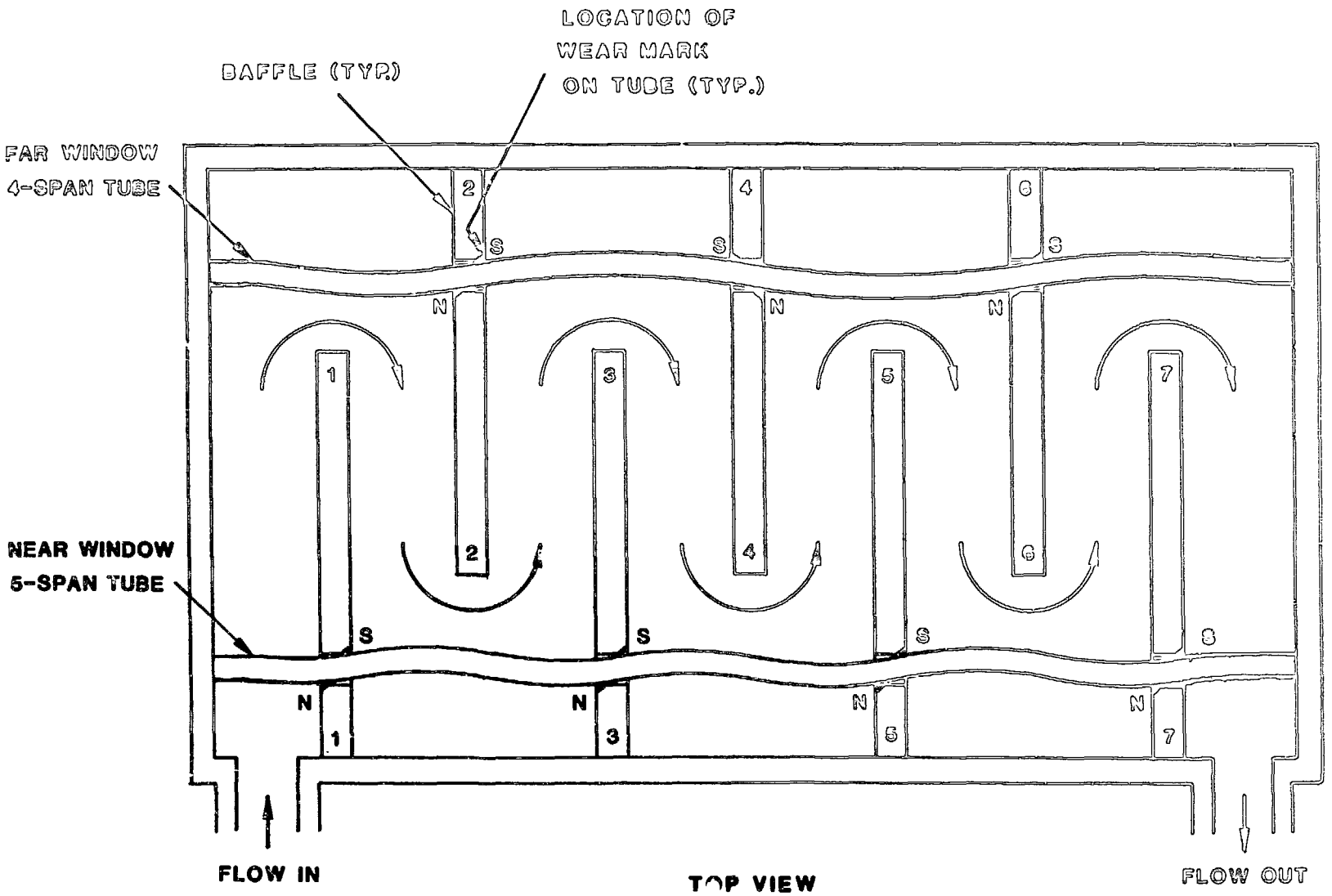

NOTE: EXAGGERATED TUBE DEFORMATION
SHOWN AS DEDUCED, NOT CONFIRMED.

Fig. 13. Post test case 17 baffle marks on window tubes

but placing them in tension (generally an advantage) as the pressure drop is applied.

Case 19

Case 19 is a 6-crosspass (5-baffle), full tube bundle configuration with 14 inch size inlet/outlet nozzles. To obtain a typical industrial configuration, as advised by HTRI, one tube row was cut from the baffles to increase the baffle cut from 25.5 to 29.6 percent. Thus the baffle edge was located near the center of the "saddled" rows G and Q. The flowrate dependent tube vibration response differed in various regions of the test exchanger as described below. Principal test results are given on Table 4.

Fluidelastic instability initiated in the central region of tube rows R and S next to the baffle edge in the "far" window opposite of the inlet and outlet nozzles at a flowrate as low as 0.101 m^3/s (1600 gal/min). In one instant the instability initiated after several minutes of running at that constant flowrate but did not continue and ceased after a while. The instability went in and out also at slightly higher flowrates. This probably indicates that the initiation/cessation is very sensitive to minor transients. It took a minimum flowrate of 0.106 m^3/s (1680 gal/min) to permanently lock in the instability. Typical vibration frequencies were near 20 Hz as expected from calculation. Hysteresis effects were small, if not absent altogether; with decreasing flow the instability ceased at a minimum of 0.097 m^3/s (1540 gal/min).

The vibration response of tubes in the bottom region (near the shell periphery) in the rows near the baffle cut in the "far" window was somewhat different than that of the central tubes. Here the vibration amplitudes increased more gradually with increasing flowrates. Specifically monitored were the very bottom tubes designated R-21 and S-21. Even though tube R-21 is located in the row R adjacent to the baffle edge, tube S-21 one row further away from that edge was subjected to larger vibration amplitudes which rose suddenly at about 0.137 m^3/s (2170 gal/min). Fortuitously, the vibrations caused the accelerometer to rotate into an approximate 45° direction, perpendicular to the shell surface. In this orientation, there was room for the very large vibration amplitude excursion to above 15 mm (0.60 in.) peak-to-peak that were generated at the high flowrate of 0.189 m^3/s (2990 gal/min). Since tube R-21 is exposed to more of the around the baffle edge flow than tube S-21, the possible explanation for S-21 experiencing larger vibrations is that S-21 is about 14 mm (0.55 in.) closer to the shell periphery and thus more exposed to the around-the-tube bundle bypass flow. The tubes in the corresponding top locations of rows R and S, where the baffle-to-shell and the tube bundle-to-shell clearances are larger than on the bottom, were not observed to vibrate as vigorously until higher

flowrates were reached. At higher flowrates almost all tubes in the "far" window, including those in the last row W, were vibrating strongly, if not impacting. Also, the central tubes of row Q saddled in the baffles were observed to rattle vigorously in the baffle holes. In addition, the tie bars, which serve to space and secure the baffles, were observed through the "far" window observation port to vibrate with large amplitudes.

In the "near" window, next to the nozzles, vibrations could be observed or felt with the fingertips at the tube ends at increased flowrates. Instability occurred in the central region of tube rows F and E next to the baffle ecdge at 0.157 m^3/s (2490 gal/min); the acceleration signals of the instrumented tube F-12 indicated an almost instantaneous initiation of violent excursions with hardly any vibration buildup. Upon flow reduction there was substantial hysteresis, the instability ceased at flowrates as low as 0.123 m^3/s (1950 gal/min). Up to the flowrates used 0.189 m^3/s (2990 gal/min) no significant vibration of the first rows exposed directly to the flow entering from the nozzle was observed.

Case 20

Case 20 is a 6-crosspass, full bundle configuration with 10 inch size nozzles replacing the 14 inch nozzles used for the previous case 19 tests. Comparison of the principal test results, included on Table 4, indicates performance similar to case 19. The instability initiated in the central region of tube row R next to the baffle edge in the far window opposite the nozzles at a minimum flowrate of 0.104 m^3/s (1650 gal/min) but was not always sustained until a flowrate of about 0.109 m^3/s (1730 gal/min) was reached. Fig. 14 shows the sharp rise of amplitude at the critical flowrate, but frequencies are not as much influenced (Fig. 15). The spectra on Fig. 16 show a sharply tuned response near the critical flowrate. Broadband and multiple-peak spectra at flowrates lower than critical may indicate buffeting and coupling of some of the many possible response frequencies. After impacting there may be dual frequencies due to a "beating" type vibration. The bottom tubes R-21 and S-21 near the shell periphery acted much as observed and described for case 19, the gradual rise of S-21 amplitudes and frequencies are presented on Figs. 17 and 18, even the spectra in Fig. 19 remained fairly sharply tuned. A comparison of the frequency spectra from tube R-21 (Fig. 20) with the spectra in Fig. 19 indicates how tube R-21 switched into synchronism with tube S-21 when the latter, or really both, are subject to abruptly increasing amplitudes and possibly an instability threshold.

Comparison of Table 4 data shows that use of the 10 inch nozzles provided a bit more hysteresis between the initiation and ceasing instability flowrates than the 14 inch nozzles (case 19).

For the first time during the entire test program, tubes in the first row exposed to the inlet nozzle were substantially excited during case 20 testing. This occurred at a flowrate well above the onset of instability elsewhere in the tube bundle. At 0.201 m^3/s (3180 gal/min) tube A-11 was measured to have peak-to-peak amplitudes of more than 2.5 mm (0.100 in.) at 142 Hz; this is a ve severe vibration condition. At that flowrate the industrial "rho-vee-squared" value of the inlet nozzle flow was 13,000. The amplitude increase with flow rate appeared to be gradual. At the same time the neighboring tube B-11, in the second row, was excited to large amplitudes, possibly impacting, at the much lower frequency of 24 Hz, which is in the range of the commonly observed vibration frequencies for a six-crosspass configuration. At lower flowrates both instrumented A-11 and B-11 tubes vibrated with small amplitudes mainly at the higher frequencies, which increased gradually from 117 Hz at 0.126 m^3/s (1990 gal/min) up to 142 Hz.

One may recall that the near window tubes for a six-crosspass configuration have a four-span support arrangement with baffle support spaced to provide unequal spans of 0.167, 0.333, 0.333, and 0.167 portions of the total length (Fig. 4). The respective deformation curves [2] indicate that for the 1st and 2nd and to a lesser extent for the 3rd and 4th modes the relative maximum vibration amplitudes occur in the longest spans; however, in the case of the 5th and 6th modes the maximum amplitudes occur in the short spans, which are adjacent to the inlet and outlet nozzles.

Since the measured excitation of the row A and B tubes above 100 Hz indicates response at the 5th or 6th mode having the large-amplitude-in-short-span characteristic, the direct exposure of the short tube span to the inlet nozzle flow had a significant effect. Apparently this effect dominated over the much more easily excited 1st (or 2nd) mode vibrations commonly seen in the other near window tubes, as measured in row F and, at times, in row B. The severity of the high frequency vibration may be characterized in terms of g-levels: the measured 2.5 mm (0.100 in.) peak-to-peak amplitude at 142 Hz of tube A-11 corresponds to a maximum single (zero-to-peak) amplitude acceleration level of 103 g; on the other hand the theoretical 4.8 mm (0.1875 in.) peak-to-peak amplitude sufficient to initiate tube to tube impacting at first mode at about 21-Hz corresponds to a single amplitude acceleration of only 4.2 g.

Case 21

Cases 21 and 22 provided "field fixes" that were found to effectively increase the flowrate initiating instability. The fixes involve passlanes in the baffle window area created by removing tubes. The vacated holes in the baffles were left open, i.e., the basic tube bundle was not disturbed from the previous test. The holes in the tubesheet were plugged, of course.

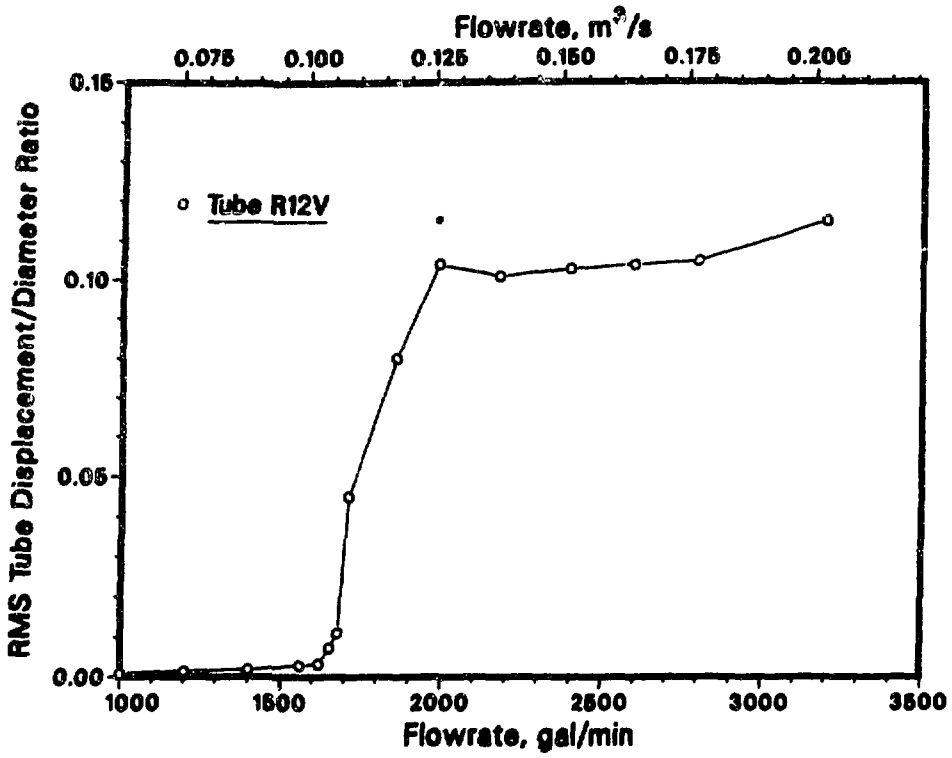

Fig. 14. RMS displacement versus flowrate: Case 20, tube R-12V

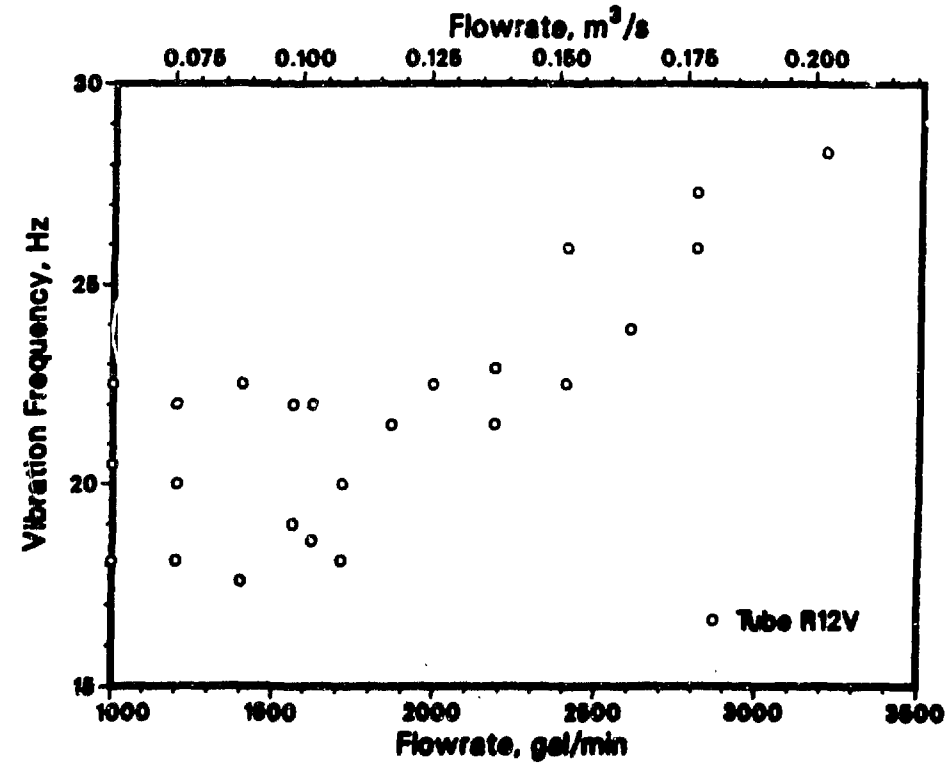

Fig. 15. Frequency versus flowrate: Case 20, tube R-12V

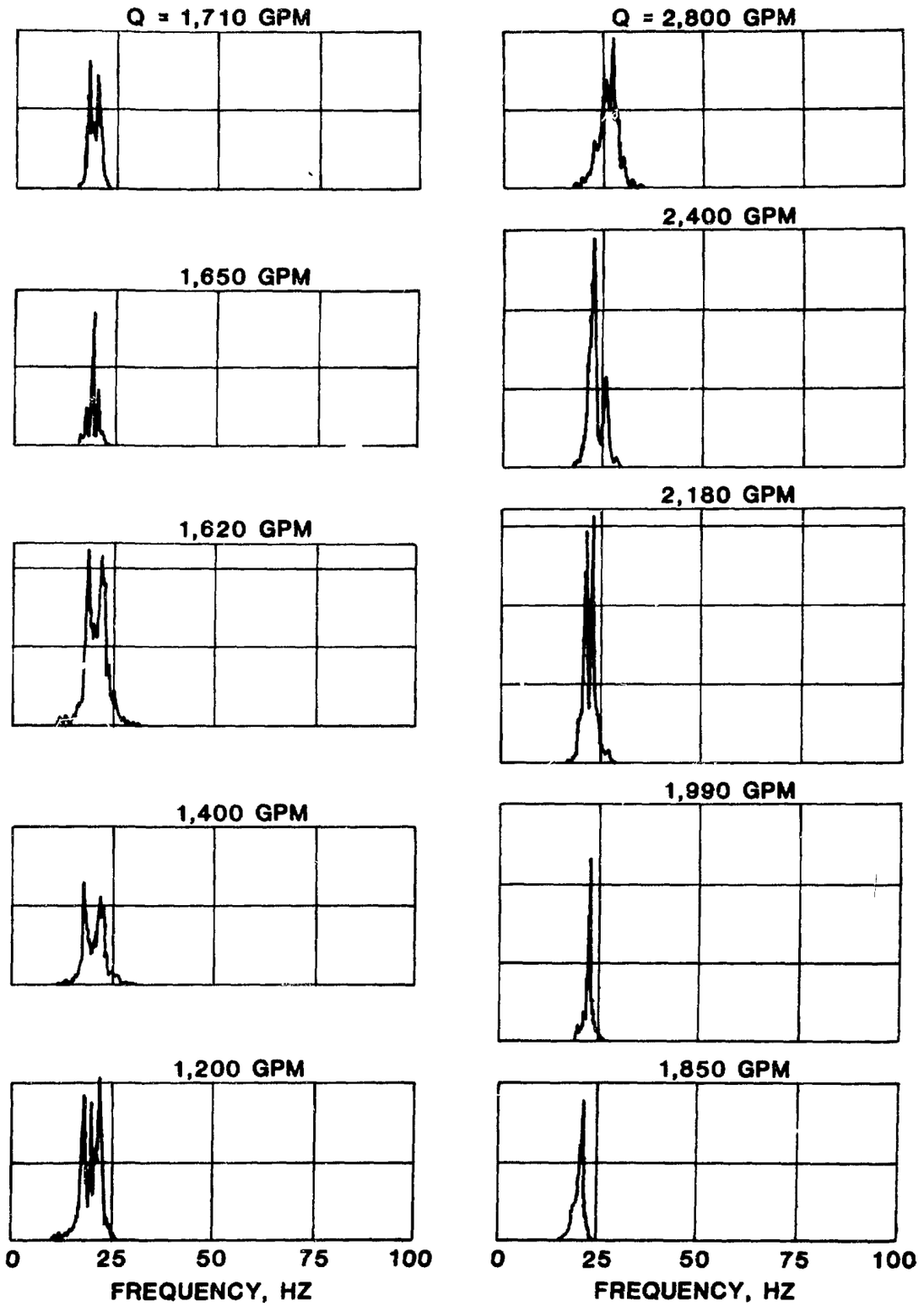

Fig. 16. Frequency response spectra: Case 20, tube R-12V

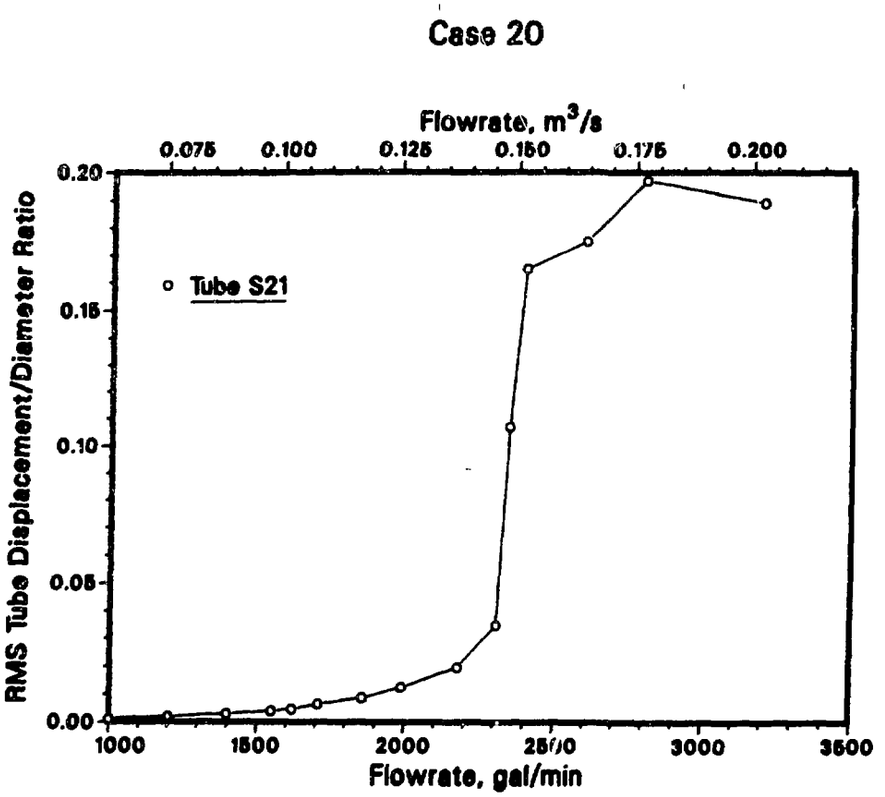

Fig. 17. RMS displacement versus flowrate: Case 20, tube S-21

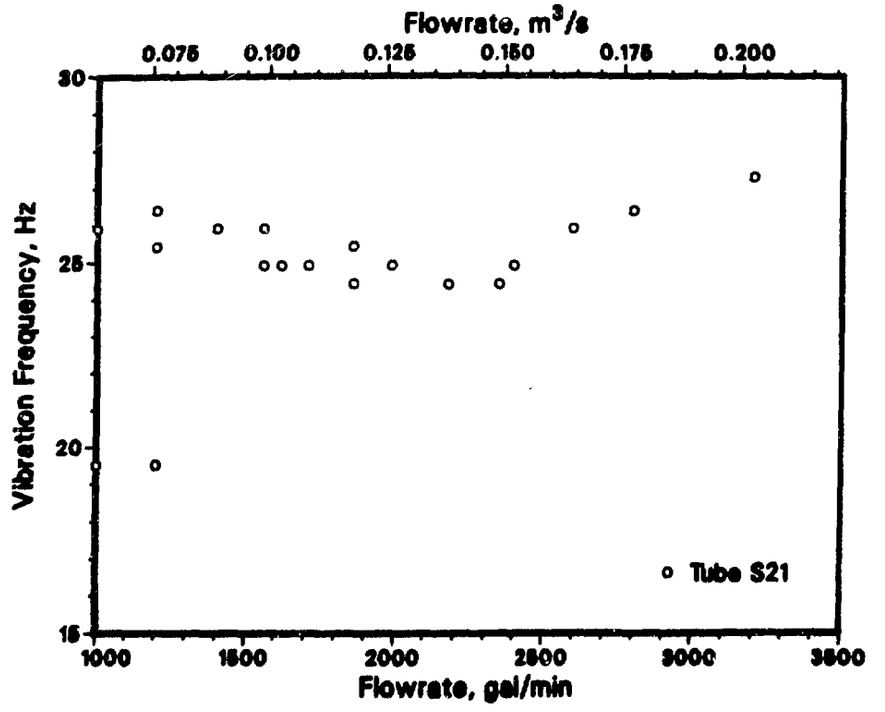

Fig. 18. Frequency versus flowrate: Case 20, tube S-21

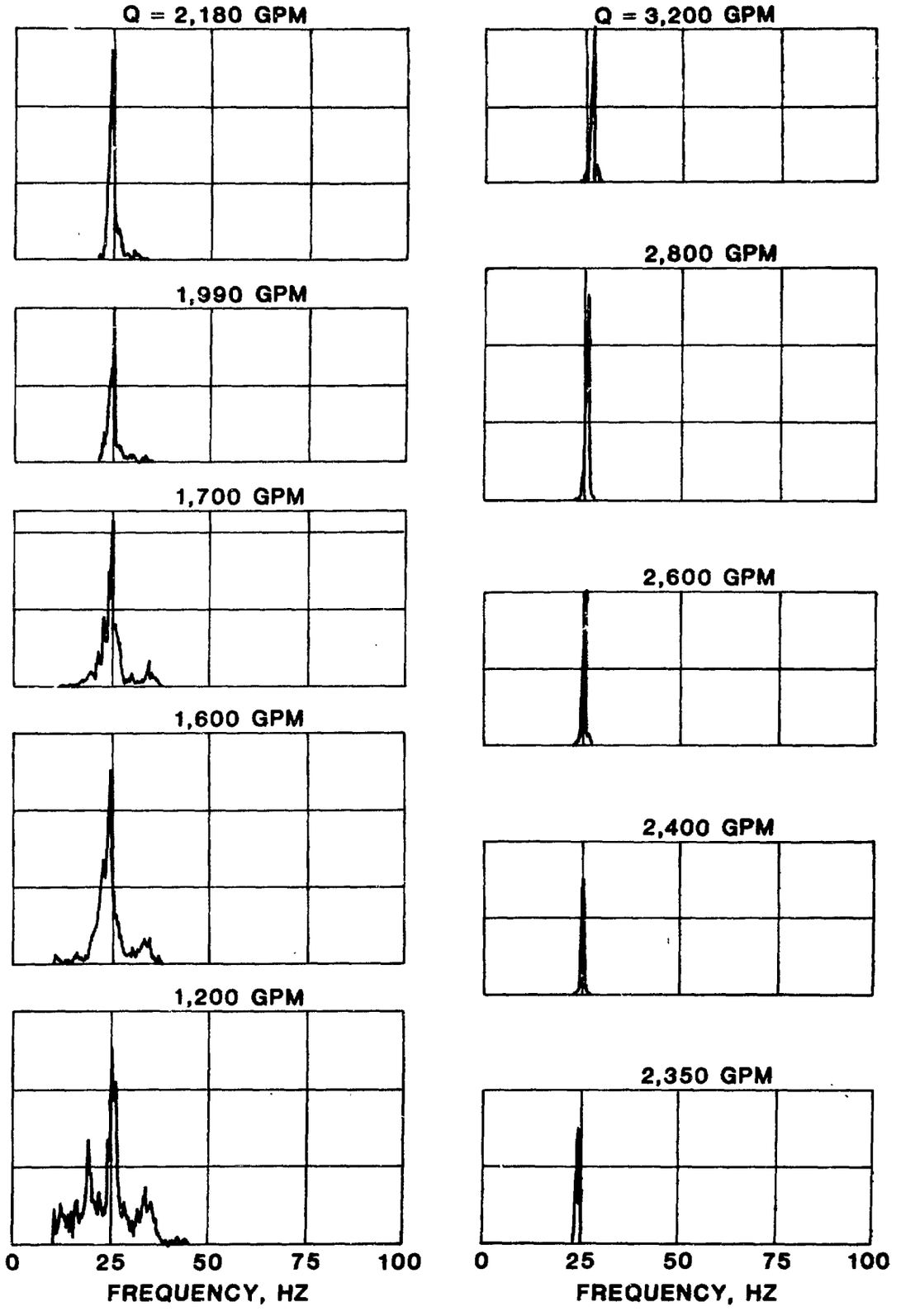

Fig. 19. Frequency response spectra: Case 20, tube S-21

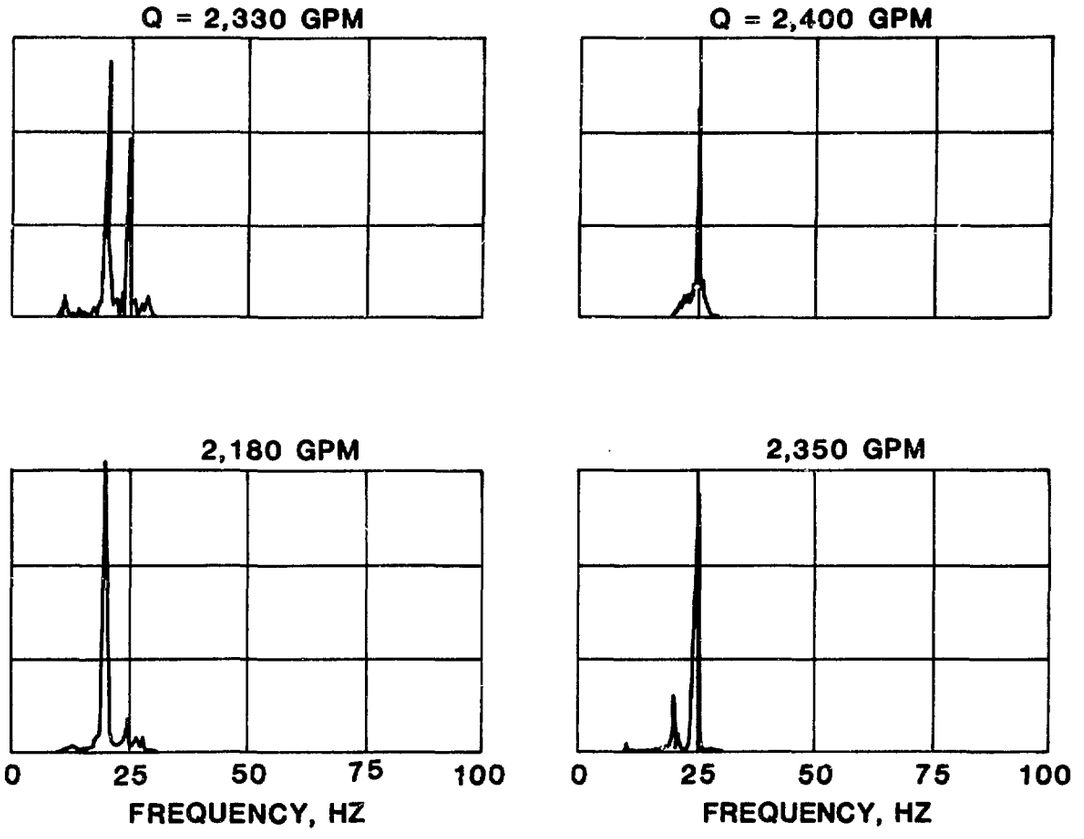

Fig. 20. Frequency response spectra: Case 20, tube R-21

This approach might be used in the field once an exchanger was found to have a vibration problem.

Case 21 is a 6-crosspass, full tube bundle configuration from which six tubes R-12 through W-12 in the far window were removed in the central plane of the test exchanger (Fig. 6b); 10 inch size nozzles were used. The instrumented tubes included R-11 and R-13, on each side of the vacated tube location R-12. The instability initiated in that central region of row R adjacent to the baffle cut at 0.122 m^3/s (1930 gal/min). This and the data pertaining to the "near" window given on Table 5 indicate how this "field fix" delayed the onset of the instability. The bottom tube of row S, S-21, next to the shell periphery in the far window incurred large, unacceptable amplitudes at about 25 Hz and probable impacting at the 0.145 m^3/s (2300 gal/min) flowrate indicated on Table 5. As discussed in the case 19 chapters, tube R-21, though less active than S-21, vibrated significantly at a lower frequency of 19.5 Hz. One test indicated that at 0.151 m^3/s (2400 gal/min) tube S-21 initiated an instability that drew tube R-21 with it into synchronism at about 25 Hz.

As will be reported later, the overall pressure drop was lowered for comparable flow rates. The heat transfer performance of the heat exchanger would also significantly decrease, but this cannot be determined with the present test set-up.

Case 22

Case 22 is a 6-crosspass, field fix, full tube bundle configuration from which 12 tubes, A-12 through F-12, as well as R-12 through W-12 were removed, thus providing passlanes in both windows in the central plane of the test exchanger (Fig. 6d). 10 inch size nozzles were used. The instrumented tubes included R-11, R-13, and F-11, all next to one of the passlanes, as well as R-21 and S-21. The principal test data, included on Table 5, indicate further increase (compared to case 21) of the flowrates initiating instability in the central region of the far and near windows, in rows R and S or F and E, at 0.132 m^3/s (2100 gal/min) or 0.223 m^3/s (3530 gal/min), respectively. It was particularly noted that tubes R-11 and R-13, straddling the passlane at the vacated R-12 position, did not always act together to go into or out of instability.

The comparison of the case 21 and case 22 test results (Table 5) with those of the full bundle case 20 (Table 4) shows that the field fixes were effective in delaying the onset of instability. This had also been the case for the corresponding 30° triangular tube pattern layout tests, as may be seen by comparing case 10 and 12 with case 7 results listed on Table 7 in a later chapter.

Case 23

Case 23 is a 6-crosspass (5-baffle) configuration with 10 inch inlet/outlet nozzles and with all tubes in both window regions, rows A through F and R through W removed to provide a no-tubes-in-window (NTIW) configuration (Fig. 6c). The unused baffle holes were covered and the tubesheet holes plugged and sealed. With all remaining tubes supported or saddled with six relatively short 0.60 m (23.5 in.) spans, no instability or even large vibration amplitudes could be observed. However, at the highest flowrate used, 0.252 m^3/s (4000 gal/min), the tubes were excited to substantial rattling within the about 0.4 mm (0.016 in.) diametral baffle hole clearances, some to levels that may not be acceptable. Such rattling response had not been observed for comparable flowrates during the testing with the 30° triangular pattern tube bundle. At the higher flowrates there was substantial vibration of the exposed tie bars used to space the baffle plates.

Because of the severe rattling observed during the initial tests, four tubes (G-9, H-9, H-10, and Q-11) were instrumented for a second test with accelerometers located midspan of the second span from the inlet end. The test results showed rms amplitudes up to 0.13 mm (0.0063 in.) indicative of additional deformation beyond the tube-in-baffle-hole motion. The vibrations occurred at or near the expected 65 Hz frequency for the six-span tube support configuration. Again the exposed tie bars were subject to severe vibration. Further discussion is presented under case 18.

Case 24

Case 24 incorporates a design fix called FIVER (Flow-Induced Vibration Evasion Restraint) into a six-crosspass, full tube bundle configuration with 10 inch nozzles corresponding to case 20. The case 24 FIVER, conceived by J. M. Chenoweth, Heat Transfer Research, Inc. (HTRI), provides twelve partial baffle plates, two for each of the six crosspasses, that tie two additional tube rows in the window regions to well supported tubes in the central core of the heat exchanger. The design is shown on Figs. 21 and 22. It is seen that the effect of the partial FIVER baffle plates is to provide additional support or saddling for tubes in rows F, R, E, and S, thus leaving rows D and T as the four- and three-span tube rows next to the baffle cuts, i.e., the first rows not secured by the FIVER baffles.

Indeed the test results indicate that the fluidelastic instability initiated in the central "far" window region of the tube row T next to the baffle edge of the FIVER. There was considerable variation of the threshold flowrate, the lowest minimum observed was 0.177 m^3/s (2800 gal/min) (Table 5). Upon decreasing flow, the instability ceased at 0.167 m^3/s (2640 gal/min). Thus the FIVER resulted in a 70 percent increase of the critical

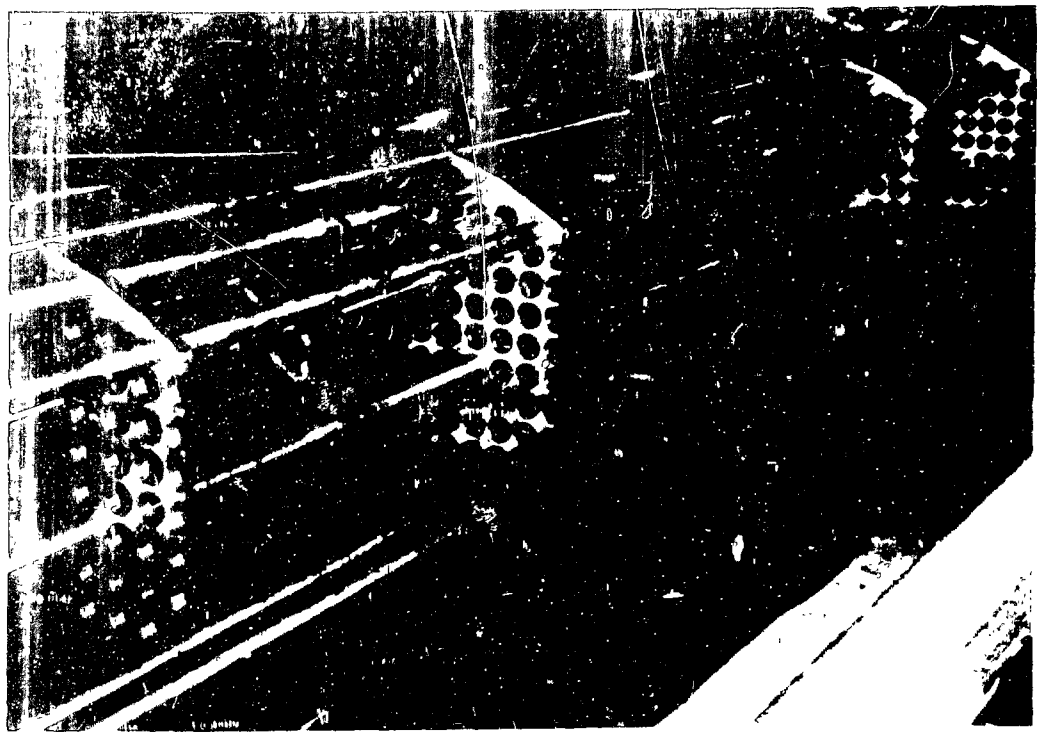

(a)

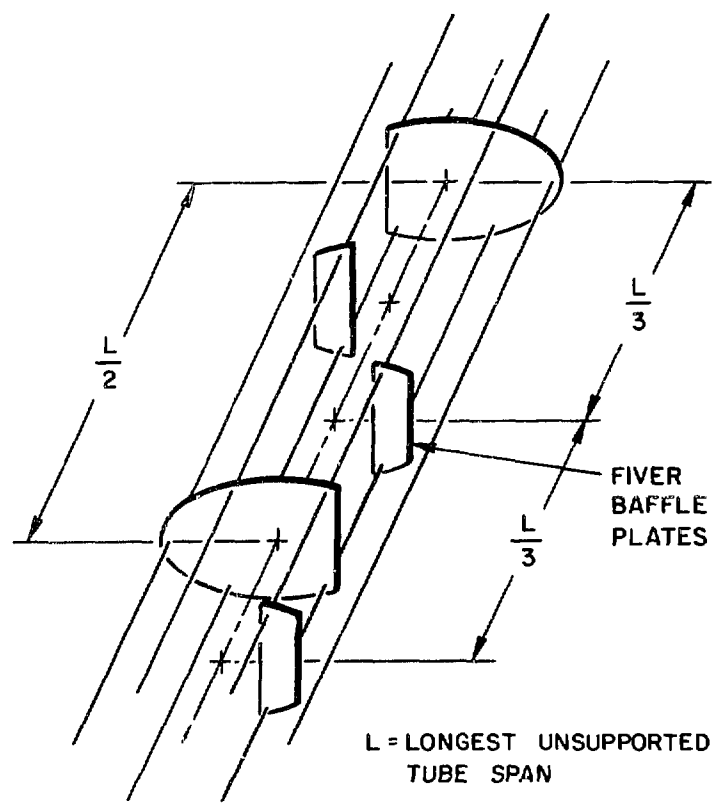

(b)

Fig. 21. Arrangement of FIVER baffles: (a) Photograph taken during assembly of tube bundle, (b) Schematic

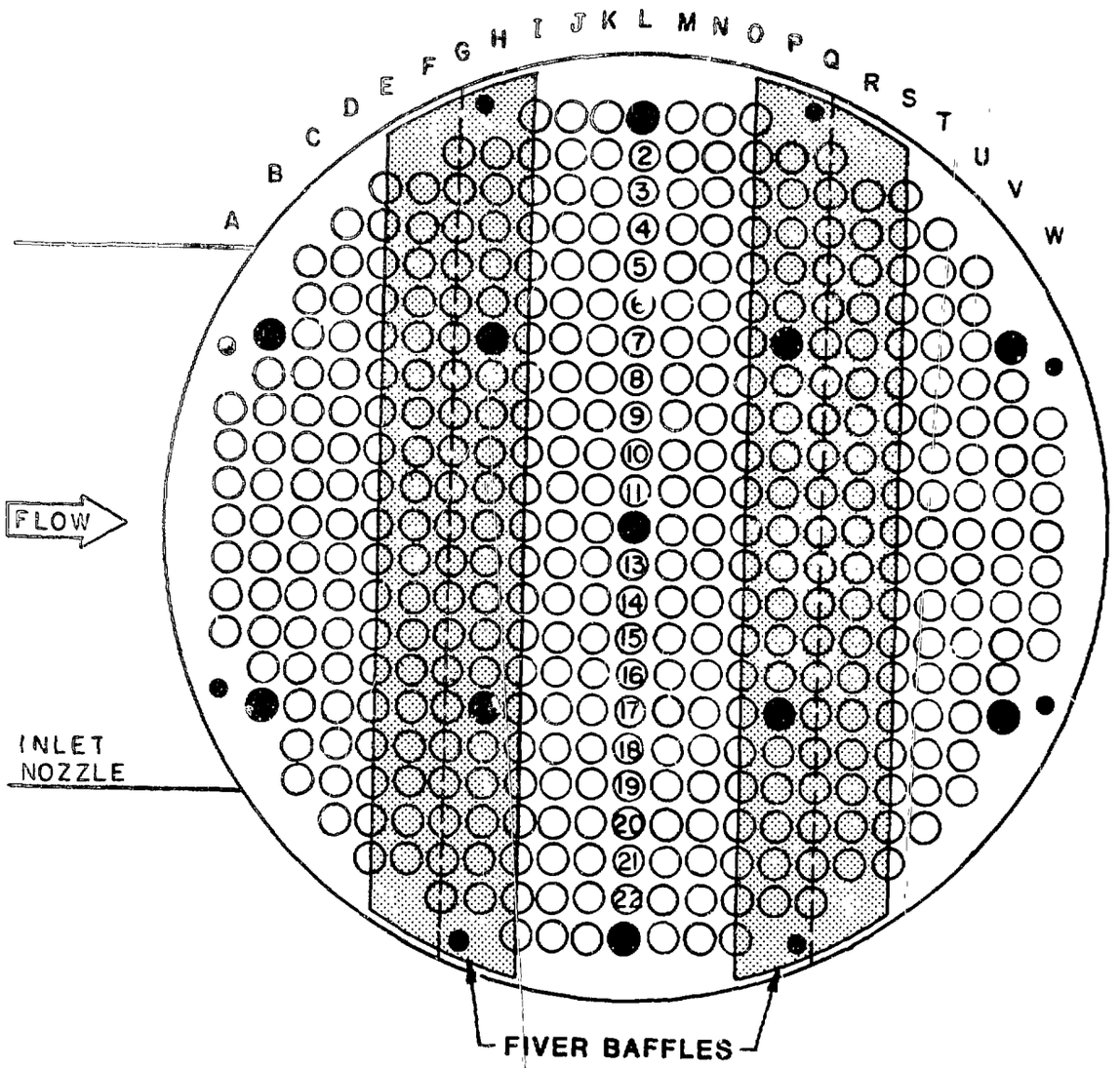

Fig. 22. Tube layout indicating positions of FIVER baffles

flowrate compared to the 0.104 m^3/s (1650 gal/min) value determined for the base case 20 tube bundle with an approximately 10 percent increase in pressure drop. However, this advantage can probably not be realized in the tested configuration with 10 inch inlet/outlet nozzles for reasons explained below. Prior to reaching the 0.177 m^3/s (2800 gal/min) threshold, the tubes in the "near" window next to the nozzles became subject to high frequency "buzzing" that built up into severe vibrations, particularly in tube row A exposed to the nozzle, as the flowrate was increased to 0.213 m^3/s (3380 gal/min). At this time it is not possible to determine at what flowrate the "near" window tube buzzing reaches an unacceptable level because there no definite criteria are available: the 0.151 m^3/s (2400 gal/min) level is a rough preliminary estimate based on judgment rather than on engineering evidence. Thus the performance of this particular configuration was limited by vibration of the "near" window tubes before tube instability in the "far" window initiated. It is expected that, if required, the vibration of these "near" window tubes can be significantly reduced by reducing inlet velocities with the use of larger nozzles.

Case 25

Case 25 is a full tube bundle of finned tubes in a 6-crosspass configuration with 10 inch nozzles. The finned tubes have plain lands at both ends and where the tubes pass through the baffle plates. Diametral dimensions are given on Table 2. There are 19 fins per inch with an approximate fin thickness of 0.51 mm (0.020 in.) and gap between fins of 0.84 mm (0.033 in.).

The finned tubes present a mixture of effects depending on the flow orientation. Even if one accepts the "squashed" diameter as the effective diameter of the finned tube, this is strictly true only for crossflow. Parallel flow encounters the over-the-fins diameter. The actual combination of cross- and parallel flow in the flow turnaround window aras thus presents a complex situation with gap dimensions and pitch-to-diameter ratio also being affected.

The flow testing of the finned tube bundle indicated sharply tuned response with small or moderate amplitudes of the central tubes in the rows R, S, and F next to the baffle edges at flowrates below those associated with impacting. The vibration amplitudes increased gradually with flowrate from about 0.5 mm (0.020 in.) rms at 0.118 m^3/s (1870 gal/min) for tube R-12 (and less for R-13 and S-12) to about 0.9 mm (0.035 in.) rms at 0.147 m^3/s (2330 gal/min) when impacting initiated. Note also sensory observations presented in Appendix. Similarly the instrumented tube F-11 in the near window indicated a sharp frequency response at the same lower flowrate with about 0.07 mm (0.0027 in.) rms amplitude but did not commence impacting

until 0.188 m^3/s (2980 gal/min) was reached. Also, the peripheral tube T-20 indicated sharp spectra at 0.154 m^3/s (2440 gal/min) but did not impact at the highest 0.226 m^3/s (3590 gal/min) flowrate tested. In both cases, the sharp frequency response is indicative of instability. It may be noted that even though the accelerometers were located and oriented - as previously discussed - at the location and in the sensitivity direction expected to experience the largest amplitudes, this may not necessarily have been the actual case upon testing. Also, the actual peak-to-peak amplitudes are higher than the theoretical 2.83 multiple (for pure sinusoidal vibration) of the measured rms amplitudes. Thus the determination of the critical flowrate requires some engineering judgment and discretion. The data presented on Table 5 correspond to the onset (or cessation) of impacting.

As the flowrate was increased, the instrumented tube A-11 in the first row exposed to the inlet flow responded at various first and higher mode frequencies. At 0.226 m^3/s (3590 gal/min) the first row tubes went abruptly into a violent vibration instability that damaged the accelerometer installation in tube A-11 within 10 seconds. Post-test examination of tubes that had been located in row A under the nozzle indicated that some had been subjected to noticeable wear in the tube holes of the baffle adjacent to the inlet nozzle. This wear, nominally about 0.08 mm (0.003 in.) diametrical, was apparently caused during operation, with a violent instability initiated at a flowrate well above the critical flowrate for instability in the "far" window section opposite the nozzles.

Case 26

Case 26 is a finned tube bundle in a 6-crosspass configuration with 10 inch nozzles and with all tubes in both windows removed to provide a no-tubes-in-window configuration, with essentially the same set-up as described for the plain tube test case 23 (Fig. 6c). During the flow testing, flowrates up to 0.332 m^3/s (5270 gal/min) were applied, but no instability or large vibration amplitudes could be observed. At the higher flowrates the tubes were felt to vibrate at a frequency estimated to be about 60 Hz, resulting in a buzz effect on the fingertips as described in the summary of sensory observation. As during previous NTIW tests, the tie bars exposed by the removal of the window tubes were subjected to severe vibration at lower flowrates. Further discussion is presented under case 18.

V. TEST PROGRAM OVERVIEW

One of the basic objectives of the Heat Exchanger Tube Vibration program is to evaluate the data from the subject test work - in conjunction with data from the collected field experiences [6-9] - to improve current predictive methods and design guidelines. This section presents the initial

efforts toward this goal. The aim is to present the test data in such a manner to not only facilitate a more complete evaluation to be performed later under this program but also to permit researchers in the future, beyond the end of the program, to utilize the "raw" data to apply the then available state-of-the-art methods not only for vibration performance per se but also for the definition and determination of significant parameters such as a characteristic flow velocity or the effective hydrodynamic mass coefficient. Table 6 presents a test matrix facilitating cross reference of all 25 different cases tested to date. The details of cases 1-5 and 6-16 were presented in [1] and [2] respectively. Tables 7 and 8 present critical flow velocities of the 30° triangular layout and the 90° square layout testing covered herein, respectively. The determination of the flow velocity is discussed below.

As a result of the testing performed to date, it has been demonstrated that different groups of tubes first experience fluidelastic instability at different flowrates. For example, the testing has shown that in general the tubes in the central portion of the row immediately adjacent to the baffle cut in the far window region experience instability first, as flowrate is increased, while the near window tubes do not go unstable until a significantly higher flowrate is reached. However, there are cases in which specific tubes (for example case 16, tube S-21) experience instability at a unique flowrate. This variance can be directly attributed to the fact that the flow pattern within the heat exchanger is very complex as the result of the baffling and the leakage paths between tube bundle and shell and through the tube-to-baffle clearance. The complex flow pattern gives rise to a highly nonuniform distribution of the crossflow, along the length of any given tube, that also varies in magnitude from tube to tube.

The crossflow velocity is one of the most significant parameters influencing the vibration performance of heat exchanger tubes. In laboratory tests with uniform crossflow, most researchers consider the mean crossflow velocity in the gap between the tubes to be "the" characteristic flow velocity; this velocity can be easily calculated in such situations. However, in a real heat exchanger the complex flow patterns and nonuniform axial distribution makes the determination of a characteristic crossflow velocity a challenge. Obviously, a single value for crossflow is not sufficient to predict instability when different groupings of tubes undergo instability at different flowrates. Experimental determination presents difficulties considered beyond the scope of the present program as discussed in Reference [1]. An effort to determine the required flow velocities by means of flow distribution computer programs has been initiated [10]. These programs have the potential of calculating not only the velocity in the pure crossflow regions but also in the window flow-turnarounds, where the tubes subject to instability are located.

It is recognized, as discussed above, that, in general, a single value of crossflow velocity is not adequate to predict the onset of instability in the various regions of a tube bundle. However, without resorting to a sophisticated three-dimensional code, or an expensive test program, the best one can do is to calculate a mean crossflow velocity, representative of the bundle, accounting, as possible, for the various leakage paths. It should also be noted that the designer is primarily interested in the lowest critical flowrate as it is the flowrate he must design to avoid. Consequently, there is an interest in developing an empirical relationship for predicting the lowest critical flowrate based on a single-value mean crossflow velocity for a particular bundle configuration.

For the present analysis, the crossflow velocity is computed from the overall flowrate through the heat exchanger by means of the HTRI computer program ST-4 [11]. The calculation is influenced by the flow diverted from the subject tube gaps due to leakage through various bypass paths: around the tube bundle, and through tube/baffle hole and baffle/shell clearances. These leakage flows depend on the pressure drops experienced across the various internal sections of the heat exchanger. The measurement of such pressure drops is hoped to provide feedback information relative to the use of the computer program. Minor changes of the velocity information in Table 7 compared to References [1] and [12] are the consequence of updated HTRI computer programming. The listed critical flow velocities correspond to the lowest critical flowrates encountered. As noted on Tables 7 and 8, no instability was found for the no-tubes-in-window bundles within the range to the highest flowrate listed.

Table 9 lists pairs of corresponding test cases to facilitate comparison with respect to the four pairs of different parameters listed: layout, nozzle size, number of crosspasses, and tube type. The paired data readily permit the computations of data ratios; it is anticipated that these ratios and the factors that influence them will be more closely investigated under this program in the future.

The application of flow induced vibration criteria generally requires knowledge of the damping and virtual mass of the tubes. The determination and use of these parameters requires discretion. In the past, both in-air and in-water values have been used, sometimes separately and sometimes in combination. While the majority of the investigators have used in-water values, Chen [13,14] has recently proposed the use of in-air values as a means to avoid the ambiguity of which coupled mode frequency and associated added mass coefficient to use. In the following, the in-water parameters are utilized. However, in a subsequent discussion, in-air values are also given for comparison.

Table 6. Matrix of flow tests

Identification by Case Number

Crosspasses Tube Type Tube Bundle Feature	Nozzle Size in.	8 Plain Full	8 Plain NTIW	6 Plain Full	6 Plain NTIW	6 Plain Fix Pass-lane(s)	6 Plain Fix Special	6 Finned Full	6 Finned NTIW
30° Triangular	10	3	4	7,11	13	10,12	8,9	15	14
	12	2							
	14	1	5	6					
90° Square	10	16		20	23	21,22	24	25	26
	14	17	18	19					

Table 7. Critical flow velocities of 30° triangular layout heat exchanger configurations

Case	No. of Cross-passes	Tube Bundle Configuration	Nominal Size Nozzles in.	Lowest Critical Flow Rate m^3/s	(gal/min)	Computed Crossflow Velocity, U m/s	(ft/s)	Typical Vibration Frequency, f Hz	Reduced Velocity** $\bar{U}$
1	8	Full	14	0.205	(3250)	2.64	(8.67)	32.2	4.31
2	8	Full	12	0.201	(3190)	2.59	(8.51)	33.7	4.04
3	8	Full	10	0.197	(3130)	2.54	(8.35)	37.1	3.60
4	8	NTIW*	10	0.317*	(5030)*	4.08*	(13.4)*	119.0	1.80*
5	8	NTIW*	14	0.316*	(5010)*	4.08*	(13.4)*	119.0	1.80*
6	6	Full	14	0.125	(1980)	1.33	(4.37)	20.5	3.41
7	6	Full	10	0.124	(1970)	1.32	(4.35)	21.0	3.31
8	6	Field Fix***	10	0.107	(1700)	-	-	~21	-
9	6	Fix†	10	0.155	(2450)	1.64	(5.38)	~21	4.10
10	6	Field Fix††	10	0.164	(2600)	-	-	~21	-
12	6	Field Fix†††	10	0.181	(2870)	-	-	~21	-
13	6	NTIW*	10	0.284*	(4500)*	3.00*	(9.84)*	67 est.	2.35* est.
14	6	Finned-NTIW*	10	0.394*	(6250)*	2.81*	(9.23)*	60 est.	2.77* est.
15	6	Finned-full	10	0.202	(3200)	1.43	(4.69)	~18	4.69

*No instability encountered at highest flowrates to which NTIW (No-tubes-in-window) configuration was subjected

**$\bar{U} = U/fD$; D = 19.1 mm (0.75 in.) O.D. for plain and 16.9 mm (0.666 in.) "squashed" diameter for finned tubes

***Tubes in row U removed

†Tubes in row U replaced by stainless steel tubes

††Horizontal passlane created by removal of 11 tubes in Rows U through AA, Nos. 23 and 25 or 24 as applicable

†††As †† with additional 11 tubes removed in rows A through G, Nos. 23 and 25 or 24 as applicable

Table 8. Critical flow velocities of 90° square layout heat exchanger configurations

Case	No. of Cross-passes	Tube Bundle Configuration	Nominal Size Nozzles in.	Lowest Critical Flow Rate* m^3/s	(gal/min)	Computed Crossflow Velocity, U m/s	(ft/s)	Typical Vibration Frequency, f Hz	Reduced Flow Velocity*** $\bar{U}$
16	8	Full	10	0.148**	(2340)**	2.12	(6.95)	32.7	3.40
17	8	Full	14	0.149**	(2360)**	2.13	(7.00)	32.7	3.43
18	8	NTIW*	14	0.303*	(4800)*	4.38*	(14.4)*	120 est.	1.92* est.
19	6	Full	14	0.101	(1600)	1.17	(3.83)	20.5	2.99
20	6	Full	10	0.104	(1650)	1.20	(3.95)	20.5	3.08
21	6	Field Fix††	10	0.122	(1930)	-	-	19.0	-
22	6	Field Fix††	10	0.132	(2100)	-	-	19.0	-
23	6	NTIW*	10	0.252*†	(4000)*†	2.96*	(9.74)*	66	2.36*
24	6	Design Fix (FIVER)	10	0.177†††	(2800)†††	-	-	21.5	-
25	6	Finned-full	10	0.147	(2330)	1.15	(3.77)	18.1	3.75
26	6	Finned-NTIW	10	0.332*	(5270)*	2.70*	(8.86)*	60 est.	2.66* est.

*No instability encountered at highest flowrates to which NTIW (No-tubes-in-window) configuration was subjected.

**Unacceptable tube vibration performance - with local instability - encountered at lower flowrate: Case 16: 0.144 m^3/s (2280 gal/min); Case 17: not precisely determined, but not less than 0.124 m^3/s (1960 gal/min), see text.

***$\bar{U} = U/fD$; D = 19.1 mm (0.75 in.) for plain and 16.9 mm (0.666 in.) for finned tubes

†Probably unacceptable tube rattling at this flowrate.

††Case 21: Horizontal passlane created by removal of 6 tubes R-12 through W-12;
Case 22: As Case 21 with additional passlane created by removal of 6 tubes A-12 through F-12.

†††Unacceptable tube vibration performance - in other regions of bundle - encountered at lower flow rates: not well determined, about 0.151 m^3/s (2400 gal/min), see text.

Table 9. Comparison of pairs of corresponding test cases

Different Parameters						
	Common	8•14	8•10	6•14	6•10	6•10•F
30°/90° layout	Cases	1/17	3/16	6/19	7/20	15/25
	Q_{cr}	3250/2360	3130/2340	1980/1600	1970/1650	3200/2330
	U_{cr}	8.67/7.00	8.35/6.95	4.37/3.83	4.35/3.95	4.69/3.77
	$\bar{U}_{cr}$	4.31/3.43	3.60/3.40	3.41/2.99	3.31/3.08	4.17/3.31
	Common	8•30	6•30	8•90	6•90	
10/14 in. Nozzles	Cases	3/1	7/6	16/17	20/19	
	Q_{cr}	3130/3250	1970/1980	2340/2360	1650/1600	
	U_{cr}	8.35/8.67	4.35/4.37	6.95/7.00	3.95/3.83	
	$\bar{U}_{cr}$	3.60/4.31	3.31/3.41	3.40/3.43	3.08/2.99	
	Common	14•30	10•30	10•90	14•90	
8/6 crosspasses	Cases	1/6	3/7	16/20	17/19	
	Q_{cr}	3250/1980	3130/1970	2340/1650	2360/1600	
	U_{cr}	8.67/4.37	8.35/4.35	6.95/3.95	7.00/3.83	
	$\bar{U}_{cr}$	4.31/3.41	3.60/3.31	3.40/3.08	3.43/2.99	
	Common	6•10•30	6•10•90			
Plain/finned tubes	Cases	7/15	20/25			
	Q_{cr}	1970/3200	1650/2330			
	U_{cr}	4.35/4.69	3.95/3.77			
	$\bar{U}_{cr}$	3.31/4.17	3.08/3.31			

Legend: Common: Configuration code of common parameters; refer to nomenclature

Q_{cr}: Critical flowrate, gal/min (1 l/min = 6.309 x 10^{-5} m^3/s)
U_{cr}: Critical flow velocity (1 ft/s = 0.3048 m/s)
$\bar{U}_{cr}$: Reduced critical flow

The difficulties of determining damping have been discussed widely in the literature. For the purpose of calculations herein, the fraction of critical damping ζ will be taken to be 0.035 in water, unchanged from the value proposed in a previous test report [1] and ASME paper [12], and 0.015 in air. The value of the virtual mass was recomputed, from that used in Refs. 1 and 12, on the basis of data presented in Table 10 and discussed below. The added mass correction factor [15], required to compute in-water natural frequency and mass-damping parameter, is a function of the array pattern, the size of the array considered, and the pitch-to-diameter ratio. In effect, there is a different added mass factor corresponding to each of the coupled modes. Ideally, one should use the added mass factor corresponding to the particular mode in which the bundle goes unstable. Unfortunately, the instability mode is, in general, not known. As a compromise, the added mass correction factor is calculated for the uncoupled vibration mode which takes into account the proximity to surrounding tubes in the tube bundle but does not account for coupling with adjacent tubes (adjacent tubes are assumed to be rigid). For plain tubes and a P/D of 1.25, the added mass correction factor for the uncoupled mode and the 30° triangular layout is 1.71, while that for the 90° square layout is 1.52; for finned tubes, with a pitch-to-diameter ratio of 1.41, the corresponding factors are 1.38 and 1.26, respctively, for a 30° triangular and 90° square layout. It should be noted that these results are for a tube in the center of an array, and thus are not truly applicable for tubes on the periphery of the tube bundle. The virtual mass is obtained by multiplying the added mass coefficient by the mass of the displaced water and adding the mass of the tube. The square root of the actual over virtual mass ratio defines the reduction of the natural frequency in water compared to in air. Values of the mass damping parameter calculated both with in-air parameters and in-water parameters, corresponding to the uncoupled mode, are given in Table 10. Comparison between first mode theoretical, both in-air and in-water (uncoupled mode), and experimental tube vibration frequencies is presented on Table 11. Previous test reports [1,2] have presented information on the higher vibration modes.

VI. PRELIMINARY EVALUATION

A primary purpose of the Heat Exchanger Tube Vibration Program is to generate data for use in the evaluation and improvement of prediction methods. The earliest correlation was that developed by Connors [16], based on experimental data, and applicable to tube rows subjected to air flow. Subscquently, different correlations have been proposed. These can be divided into two groups

Table 10. Virtual mass calculation

Layout	30° Triangular		90° Square	
Tube Type	Plain	Finned	Plain	Finned
Tube Diameter, mm	19.1	16.9	19.1	16.9
in.	0.750	0.666	0.750	0.666
Pitch/Dia. Ratio	1.25	1.41	1.25	1.41
Added Mass Coefficient (Uncoupled Mode)	1.71	1.38	1.52	1.26
Array Size	37	37	25	25
Tube Mass, m_{act}, kg/m	0.597	0.656	0.597	0.656
lb/in.	0.0335	0.0367	0.0335	0.0367
Displaced Water, actual mass kg/m	0.285	0.225	0.285	0.225
lb/in.	0.0160	0.0126	0.0160	0.0126
Virtual mass, m_v, kg/m	1.09	0.965	1.03	0.938
lb/in.	0.0609	0.0541	0.0578	0.0526
Ratio: $(m_{act}/m_v)^{0.5}$	0.742	0.824	0.761	0.835
Mass Damping Parameter, δ_m				
In-air (ζ = 0.015)	0.155	0.216	0.155	0.216
In-water (ζ = 0.035)	0.659	0.742	0.626	0.721

Table 11. Theoretical and experimental vibration frequencies

Definitions: Theoretical: Calculated fundamental (1st mode) natural frequencies
Experimental: Predominant vibration frequencies encountered during flow testing.
Refer to Tables 7, 8, 10, and 13

No. of crosspasses	8	8	8	6	6	6	6
Tube location (window)	Far	Near*	Core	Far	Near*	Core	Finned Far
No. of spans	4	5	8	3	4	6	3
Theoretical, Hz							
In air, 1st mode	50.1	51.0	179.2	30.9	32.1	104.0	20.7**
In water, uncoupled mode							
30° layout	37.2	37.8	133.0	22.9	23.8	77.2	17.1**
90° layout	38.1	38.8	136.3	23.5	24.4	79.1	17.3**
Experimental, Hz							
Case Nos. in ( )							
30° layout	(1) 32.2	38.6*	(4) 119	(6) 20.5	30.8*		(15) 18
	(3) 37.1	28.0		(7) 21.0	31.3		
90° layout	(16) 32.7	29.3*		(19) 20.5	24.9	(23) 66	(25) 18.1
	(17) 32.7	34.7*		(20) 20.5	25.4		

*Near window vibration frequencies at onset of instability are often difficult or impossible to determine because of violently abrupt initiation. Data with * are estimates.

**Based on simplifying assumptions, e.g., uniform tube along length, that apparently render values somewhat low.

$$\left(\frac{U}{fD}\right) = \alpha_1 \left(\frac{2\pi\zeta m}{\rho D^2}\right)^{\alpha_2} \tag{1}$$

and

$$\left(\frac{U}{fD}\right) = \beta_1 \left(\frac{m}{\rho D^2}\right)^{\beta_2} (2\pi\zeta)^{\beta_3} \tag{2}$$

where α_1, α_2, β_1, β_2, and β_3 are empirical constants. Recent work of Chen [17] has led to an improved understanding of the fluidelastic phenomenon. Among other things, his studies have demonstrated that there are, in fact, two types of instability mechanisms possible and that a correlation of the form of Eq. (1) is applicable for gas flow, while Eq. (2) is more appropriate for liquid flow. At this time, there is not sufficient data available to evaluate the empirical constants in Eq. (2). Consequently, a stability equation of the form given in Eq. (1) is employed; additionally, a value of 0.5 is often assumed for α_2. With $\alpha_2 = 0.5$, Eq. (1) corresponds to Connors' original stability equation, which Chen has shown to be valid for high values of the mass-damping parameter, corresponding to gas flows.

In computing the reduced flow velocity U_r (= U/fD) and mass-damping parameter δ_m (= $2\pi\zeta m/\rho D^2$) either in-air or in-water parameters can be used. In Table 12, reduced critical flow velocities, based on effective crossflow velocities computed from the HTRI ST-4 code (See Tables 7 and 8) and theoretically calculated frequencies from Table 11, are given for the cases of in-air and uncoupled, in-water mode parameters. Utilizing the appropriate values of mass-damping parameter from Table 10, instability threshold constants α_1 are computed and listed in Table 12 for the various full tube bundle tests performed.

The instability threshold constant will depend, in part, on the procedure used to calculate the effective crossflow velocity from the measured critical flowrate. However, ideally one would hope that for a given tube layout the instability constant would be nearly constant for the various test cases corresponding to that tube layout. For plain tubes, the instability constant based on in-water parameters ranged from 3.74 to 4.59 for the 30° triangular layout and from 3.30 to 3.72 for the 90° square layout; values for the finned tubes were significantly higher in both cases, viz., 5.73 and 4.62, respectively. The variation in the constant for plain tubes can be attributed to the following: (1) Eq. (1) is not the theoretically correct form for the stability criterion for the case of dense fluids (liquids), (2) damping can only be estimated and can be expected to vary (possibly, significantly) from tube to tube, and (3) the HTRI ST-4 code gives only an effective (average) crossflow velocity, instability is dependent on local crossflow velocities which can be expected to vary significantly from the mean.

Table 12. Instability threshold constants computed from far window test results

Case	Configuration Code	Reduced Critical Flow Velocity		Instability Threshold Constant ($a_2 = 0.5$)	
		$(U_{CR})_v$	$(U_{CR})_u$	$(a_1)_v$	$(a_1)_u$
1	8 ◦14 ◦30	2.77	3.73	7.03	4.59
2	8 ◦12 ◦30	2.72	3.66	6.90	4.51
3	8 ◦10 ◦30	2.67	3.59	6.78	4.42
6	6 ◦14 ◦30	2.26	3.05	5.74	3.76
7	6 ◦10 ◦30	2.25	3.04	5.71	3.74
15	6 ◦10 ◦30 ◦F	4.08	4.94	8.77	5.73
16	8 ◦10 ◦90	2.22	2.92	5.63	3.69
17	8 ◦14 ◦90	2.24	2.94	5.69	3.72
19	6 ◦14 ◦90	1.98	2.61	5.03	3.30
20	6 ◦10 ◦90	2.05	2.69	5.20	3.40
25	6 ◦10 ◦90 ◦F	3.28	3.92	7.05	4.62

Subscripts v and u indicate calculation is based on in-air or in-water uncoupled mode parameters, respectively.

Nevertheless, based on Eq. (1), with $\alpha_2 = 0.5$, and the results given in Table 12, it is possible to put forth stability equations that envelope the results obtained for the two types of tube layouts and that are valid when used with crossflow velocities calculated by means of the HTRI code [11]. The following design criteria can be written:

Based on in-water, uncoupled mode parameters,

$$\left(\frac{U}{fD}\right) \leq \begin{cases} 3.7 \left(\frac{2\pi\zeta m}{\rho D^2}\right)^{0.5}, & 30^0 \text{ layout} \\ 3.3 \left(\frac{2\pi\zeta m}{\rho D^2}\right)^{0.5}, & 90^0 \text{ layout.} \end{cases} \tag{3}$$

Based on in-air parameters,

$$\left(\frac{U}{fD}\right) \leq \begin{cases} 5.7 \left(\frac{2\pi\zeta m}{\rho D^2}\right)^{0.5}, & 30^0 \text{ layout} \\ 5.0 \left(\frac{2\pi\zeta m}{\rho D^2}\right)^{0.5}, & 90^0 \text{ layout.} \end{cases} \tag{4}$$

It is interesting to note that if the criteria based on in-water parameters were combined into one, we would obtain

$$\left(\frac{U}{fD}\right) \leq 3.3 \left(\frac{2\pi\zeta m}{\rho D^2}\right)^{0.5}. \tag{5}$$

This agrees exactly with the criterion proposed by Pettigrew et al. [18] based on data from field experiences with heat exchangers.

In his recently published paper [13], Chen has assembled available experimental data from the open literature; the data are from laboratory tests. He categorized it according to tube layout geometry and, based on the improved understanding of the fluidelastic mechanisms, has proposed lower bounds to the data in both graphical and equation form. In Figs. 23 and 24, his stability diagrams for 30° triangular and 90° square arrays, respectively, are given. The data from the subject Heat Exchanger Tube Vibration Program (Tables 10 and 12) are plotted on these stability diagrams to allow for comparisons.

For both tube layouts, the data can be seen to fall within the scatter of the laboratory test data and to quantitatively agree reasonably well with them. In both cases, the stability criteria proposed by Chen are conservative and a design based on them would be safe. Pettigrew's design criterion is also included for comparisons and the data can be compared with it.

The lowest flowrate to initiate instability is of most significance, because it is this threshold that must not be exceeded to avoid damage to

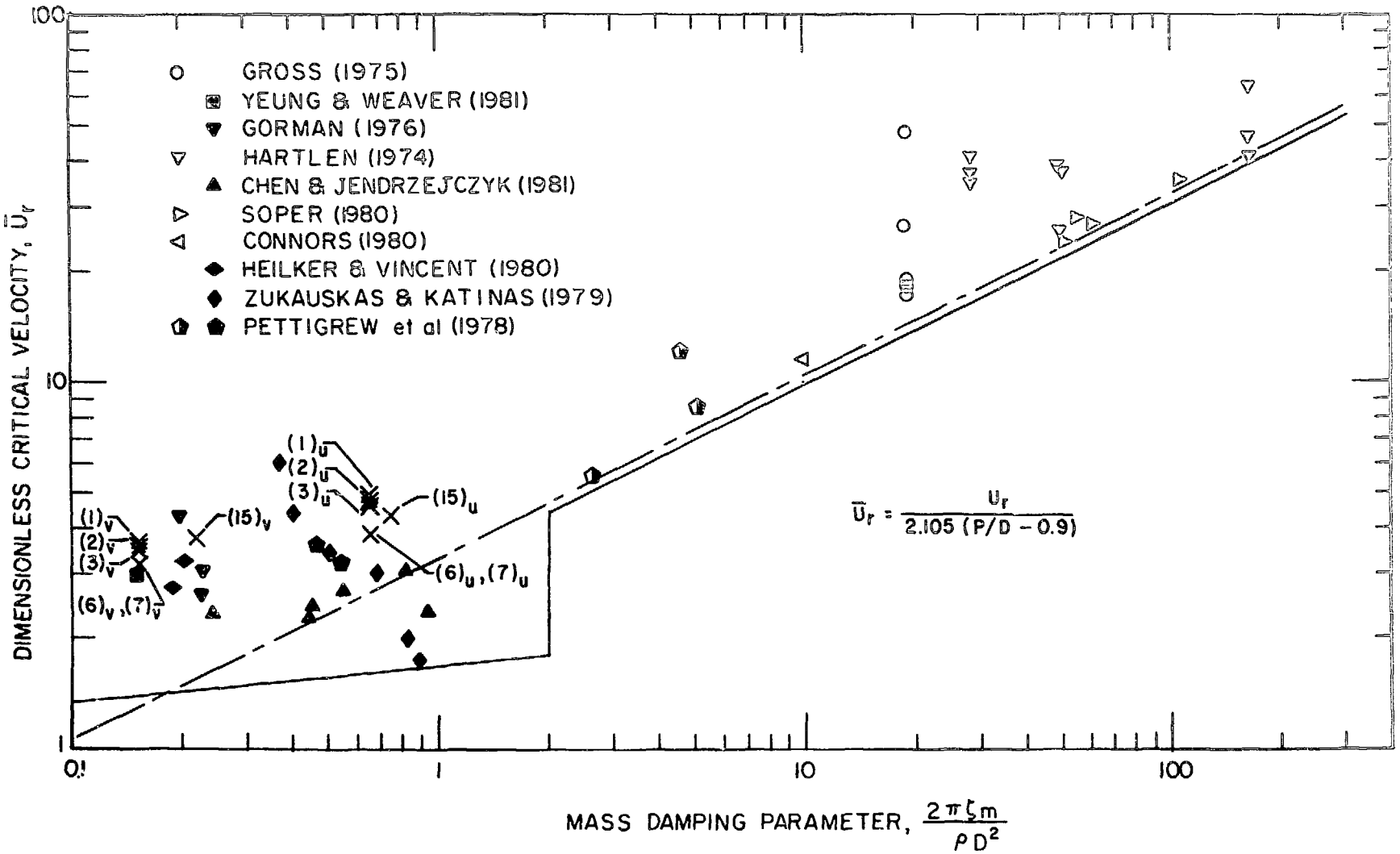

Fig. 23. Stability diagram for 30° triangular arrays [13]; comparison of heat exchanger test data with laboratory test data; ( ) defines case nos. where subscripts v and u denote in-air or in-water, uncoupled mode parameters, respectively; — - — Pettigrew's criterion [18]

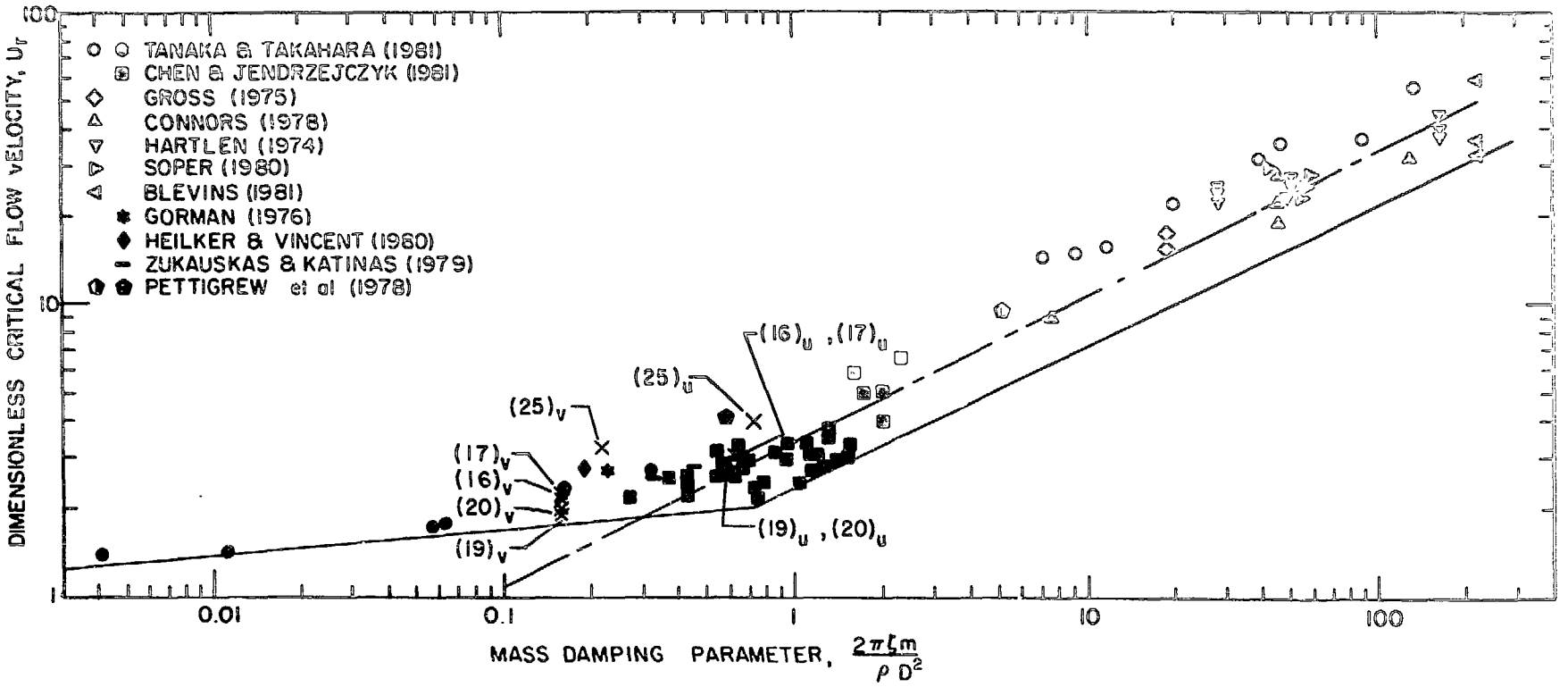

Fig. 24. Stability diagram for 90° square arrays [13]; comparison of heat exchanger test data with laboratory test data; ( ) defines case nos. where subscripts v and u denote in-air or in-water, uncoupled mode parameters, respectively; — - — Pettigrew's criterion [18]

the heat exchanger. This really provides only one data point per test. As reported, the test exchanger was exposed to much higher than critical flowrates, partly to investigate additional instabilities in the near window region. While the occurrence of these instabilities may not have much practical significance, they are of academic interest because they may provide an additional data point per test. The purpose of Table 13 is to summarize these instabilities and provide the data for evaluation parallel to those presented on Table 12. It seems that the evaluation of the vibration performance of the tubes in the near window encounters different, if not additional, complexities than those in the other regions. The higher mode high frequency excitation of row A tubes directly exposed to the inlet flow has been discussed in the case 20 report. As indicated on Table 13, the consideration of the shell entrance velocity provides a better correlation with the instability criteria for the row A tubes. At the same time the tubes, particularly those next to the baffle cut, are subject to excitation by the window turnaround flow at or near the fundamental mode frequency. At times both of these phenomena are acting on the same tube, one of them may be predominating. Even though the near window tubes have fundamental natural frequencies that are only slightly higher than those of the far window tubes (see Table 11) the reduced critical flow velocities, computed without sophistication, are much higher. This suggests that a correction for effective velocity (there is one less window) exposure should be considered. Also, when instability did initiate, it often started abruptly with violent action. Further discussion of Table 13 is probably not warranted at this time.

VII. FLOW TESTS: PRESSURE DROP

Shellside pressure drop measurements were taken for all configurations tested with room temperature water as the shellside fluid. The overall inlet to outlet pressure drop was measured between taps located on the respective nozzles by means of a differential pressure transducer. When this overall pressure drop is plotted as a function of flowrate on log-log paper, the data can be correlated with a straight line. This implies that the overall pressure drop can be correlated by a power function relationship of the general form

$$\Delta p = \gamma Q^{\alpha} \tag{6}$$

where γ and α are constants for a particular tube bundle configuration.

For this report the above equation will be expressed as

$$\Delta p(\mathrm{lb/in.^2}) = \gamma(\mathrm{lb/in.^2}) \left(\frac{Q(\mathrm{gal/min})}{1000}\right)^{\alpha} \tag{7}$$

Table 13. Instability threshold constants computed from near window test results

Case	Tube Row	Configuration Code	Instability Flowrate (gpm)	Computed Crossflow Velocity (ft/s)	Reduced Critical Flow Velocity		Instability Threshold Constant (α_2 = 0.5)	
					$(U_{CR})_v$	$(U_{CR})_u$	$(\alpha_1)_v$	$(\alpha_1)_u$
1	F	8•14•30	3430	9.14	2.86	3.87	7.26	4.77
3	F	8•10•30	3760	10.0	3.14	4.23	7.98	5.21
6	F	6•14•30	2320	5.10	2.54	3.43	6.45	4.23
7	G	6•10•30	2790	6.11	3.05	4.11	7.75	5.06
16	E	8•10•90	3480	10.3	3.23	4.25	8.20	5.37
17	E	8•14•90	3530	10.4	3.26	4.29	8.28	5.42
19	F	6•14•90	2490	5.90	2.94	3.87	7.47	4.89
20	A	6•10•90	3180	7.52	0.67†	0.88†	1.70†	1.12†
				24.9*	2.22†	2.92†	5.64†	3.69†
20	F	6•10•90	2400	5.69	2.84	3.73	7.21	4.71
25	A	6•10•90•F	3590	5.79	0.87††	1.04††	1.87††	1.22††
				27.4*	4.11††	4.93††	8.84††	5.81††
25	F	6•10•90•F	2980	4.31	4.03†††	4.81†††	8.67†††	5.66†††

Subscripts v and u indicate calculation is based on in-air or in-water, uncoupled mode parameters, respectively.

†Based on 5th mode frequency: 179.1 Hz in-air; 147.6 Hz in-water (90° layout). Experimental vibration frequency was 142 Hz.

††Based on 5th mode frequency: 120.0 Hz in-air; 100.2 Hz in-water (90° layout). Experimental vibration frequency was approximately 120 Hz.

†††Based on near window 1st mode frequency: 21.5 Hz in-air; 18.0 Hz in-water (90° layout). Experimental vibration frequency was 21.5 Hz.

*Alternate evaluation: velocity computed based on estimated shell entrance area in accordance to TEMA [3]. Flow velocity inside 10 inch nozzles is 1.38 m/s (4.53 ft/s) per 0.063 m^3/s (1000 gal/min).

1 gal/min = 6.309×10^{-5} m^3/s; 1 ft/s = 0.3048 m/s

which, taking logarithms on both sides becomes

$$\ln \Delta p(\text{lb/in.}^2) = \ln \gamma(\text{lb/in.}^2) + \alpha \ln \left\{\frac{Q(\text{gal/min})}{1000}\right\} . \qquad (8)$$

For the pressure drop data obtained from each of the various test configurations, Eq. (8) was employed to determine the constants γ and α by means of linear regression analysis. Table 14 indicates the range of flowrates from which the data were taken and summarizes the results of the linear regression analysis computations, listing, in addition to the constants γ and α, the overall pressure drops at 0.063 m^3/s (1000 gal/min) and 0.126 m^3/s (2000 gal/min). To facilitate comparison, two examples for commercial pipe, taken from an industrial catalog [19], have been included on Table 14.

In addition to the overall pressure drop the pressure drops through individual sections were measured to determine the pressure drop distribution. The entire pressure drop measurement effort and a discussion of the results are reported separately in [20]. This report includes an investigation of the exponential change (α) of pressure drop as a function of flowrate and an attempt to calculate nozzle losses.

VIII. CONCLUDING REMARKS

This investigation is motivated by the need to obtain tube vibration data from industrial heat exchanger configurations, as well as from field experiences, to contribute to the improvement of existing prediction methods for avoiding vibration damage. Previous test reports [1,2] have discussed the complexities of both the structural and the fluid dynamic phenomena encountered in investigating heat exchanger tube vibrations.

This report covers the testing of eleven different tube bundles with a 90° square layout on a 1.25 pitch-to-diameter ratio. The testing focused on identification of the lowest critical flowrate for instability. Data relating to both the sub- and postcritical vibration of the tubes were also taken. In addition pressure drop and distribution were measured. The generated data were tabulated and organized in a manner expected to facilitate present and future evaluation. For the sake of completeness and comparison, data generated during previously reported tests with 30° triangular layout pattern were included in the tabulations. Two presently available instability criteria were applied.

The principal test results and their significance for practical applications are summarized below:

1. At low flowrates, prior to any onset of instability, turbulent buffeting dominates. Examination of specific case 3, 7, 16, and 20 data showed that pre-instability rms amplitudes rise with a power slightly higher than the square of the flowrate, the exponents increase with flowrate and

Table 14. Overall pressure drop versus flowrate

$\Delta p = \gamma(Q/1000)^{\alpha}$ with U.S. units indicated††

Case	Configuration Code**	Range of flowrates Q used to determine α and γ gal/min	Exponent α	Overall pressure drop Δp at 1000 gpm γ lb/in.^{2}	2000 gpm lb/in.^{2}
1	8•14•30	770-3190	1.93	5.43	20.7
2†	8•12•30	1030-3190	1.92	5.51	20.9
3	8•10•30	800-3000	1.91	6.01	22.6
4	8•10•30•N	1175-3980	1.78	3.11	10.7
5	8•14•30•N	1580-5010	1.79	2.93	10.1
6	6•14•30	1060-2190	1.87	3.38	12.4
7	6•10•30	1160-3290	1.83	3.99	14.2
8	6•10•30•X	1100-2800	1.85	3.08	11.1
9	6•10•30•X	1600-2200	1.93	3.81	14.5
10	6•10•30•X	900-3000	1.91	3.34	12.5
12	6•10•30•X	600-3000	1.91	2.35	8.81
13	6•10•30•N	1620-4150	1.80	1.48	5.16
14	6•10•30•NF	1000-6250	1.90	1.33	4.99
15	6•10•30•F	600-2600	1.92	4.04	15.3
16	8•10•90	1000-3400	1.93	4.62	17.6
17	8•14•90	1000-2600	1.93	4.19	16.0
18	8•14•90•N	1010-3980	1.89	2.61	9.52
19	6•14•90	800-3000	1.87	2.53	9.25
20	6•10•90	1230-2790	1.95	2.77	10.7
21	6•10•90•X	600-2600	1.86	2.75	10.0
22	6•10•90•X	1190-3200	1.93	2.16	8.25
23	6•10•90•N	590-3990	1.85	1.33	4.78
24	6•10•90•X	800-2830	1.92	3.00	11.4
25	6•10•90•F	1020-3220	2.03	2.38	9.71
26	6•10•90•NF	790-5270	1.95	1.00	3.88
*	6 in. pipe	1000-2000	1.94	2.68	10.3
*	12 in. pipe	1000-2000	1.90	0.09	0.34

*Examples, 30.48 m (100 ft) of U. S. Schedule 40 pipe [19]

**Refer to nomenclature

†Use of Case 2 data requires qualifying explanation.

††1 gal/min (gpm) = 6.309×10^{-5} m^3/s
1 lb/in.^{2} = 6.895 kPa

roughly average around 2.5. The vibration response, occurring over a broad band of frequencies, typically results in small rms displacements (< 0.006 of tube diameter) and is not expected to result in tube failure. However, the effects of low level vibration on the reliability of heat exchangers designed for long lifetimes remains a concern.

2. The tube bundle can be subjected to unacceptable vibration performance at flowrates below the onset of instability for the general tube bundle. These "local" instabilities can be caused by hysteresis, leakage flow, and high inlet nozzle flow velocities as discussed in items 4, 5, and 13.

3. In general, the fluidelastic instability initiates abruptly in the central regions in the tube rows next to the baffle edge in the far window, opposite to the inlet/outlet nozzles of the exchanger. The instability mode frequency is typically at or near the lowest natural frequency.

4. "Hysteresis" effects, upon flow reversal, imply that flow transients may trigger instability at flowrates below threshold encountered with increasing flow.

5. Leakage flow passing around the tube bundle, though the gap formed with the shell, is apparently contributing to the large amplitude excitation of a few tubes on the periphery of the bundle. The amplitudes increase gradually with flowrate and can result in unacceptable vibration and impacting as a result of a local instability, say, caused by skimming leakage flow (cases 16 and 17). Such local instability can occur at flowrates below the instability threshold of groups of tubes in the central region of the bundle. Since leakage and bypass flows may result in conditions, such as creating high flow velocities through low resistance gaps or encountering a 45° layout orientation on a 90° layout bundle, the application of routine theory or laboratory type test results requires discretion.

6. Comparison indicates that the 30° triangular layout tube bundles tested are less susceptible to vibration excitation than the 90° square layout bundles. The critical flowrate advantage of eight versus six crosspass bundle was slightly greater for the 30° than for the 90° layout pattern.

7. Within the range of parameters tested, nozzle size has little effect on the onset of instability. Nevertheless, it appeared that with the smaller 10 in. nozzle the hysteresis effects were increased. On the other hand, nozzle size is significant because the smaller nozzle size results in higher entrance velocities and is considered responsible for unacceptable tube rattling and high frequency buzzing that otherwise would not have occurred at the flowrates experienced. Usually these effcts occur at flowrates higher than the critical, but there are exceptions such as NTIW case 23 and the FIVER fix case 24.

8. None of the no-tubes-in-window (NTIW) configurations experienced fluidelastic instability within the range of flowrates tested, considered to reach well beyond the flowrate practical for industrial operation. One NTIW bundle (case 23) was subjected to substantial rattling at such unreasonably high flowrates, the small inlet nozzles were apparently a factor.

9. During all NTIW tests the tie bars, weaker than the tubes and exposed to open flow, were excited to substantial vibration. Some vibration also occurred at high flowrates during other tests, e.g., cases 19, 21, 22, and 24. The significance is that the design and location of such auxiliary hardware cannot be neglected. Some considerations are presented in the case 18 test discussion.

10. The passlane field fixes (cases 21 and 22) effectively delayed the onset of instability. Any overall evaluation has to consider the loss of heat transfer surface that may be, at least partially, compensated for by higher flow velocities made possible by reduced pressure drop losses.

11. The design fix FIVER (case 24) provided a large increase in the critical flowrate with a small additional pressure drop.

12. The pressure drop information generated by these tests is expected to be useful for analyzing heat exchanger flow performance and has provided some interesting insights [20].

13. Where possible, the onset of instabilities in the near window next to the nozzles at flowrates above those initiating the far window tubes has been investigated. Even though these data do not have immediate practical importance, the results may be useful as an additional instability criteria test point from any given test.

14. The evaluation of the finned tube bundle performance is additionally complicated by the difference of cross- and parallel flow path conditions and by a more gradual rise of amplitude prior to impacting as discussed under case 25.

ACKNOWLEDGMENTS

This work was performed as part of a Heat Exchanger Tube Vibration Program which is sponsored by the U. S. Department of Energy, Office of Energy Systems Research, under the Energy Conversion and Utilization Technology (ECUT) Program, and represents a U.S. contribution to the International Energy Agency (IEA) Program of Research and Development on Energy Conservation in Heat Transfer and Heat Exchangers. The continuing encouragement and support of W. H. Thielbahr, J. J. Eberhardt, and M. Gunn of the US/DOE are appreciated.

The following people deserve acknowledgment for their help, at one time or another, with the setup and conduct of the tests and/or the processing of the data: W. A. Ellis, D. M. Engel, J. V. Killelea, R. K. Smith, and

R. A. Zolecki, also the diligent student-aides T. S. Chmelik, J. K. Roberts, and E. Zywicz.

The authors also gratefully acknowledge the assistance of J. Kissel and D. Fijas of American Standard for consultation on the layout and fabrication of the 90° square pattern tubesheets and baffles; J. G. Withers of Wolverine Tube Division, UOP, Inc., for keeping the finned tubing available for testing; and last, but not least, J. M. Chenoweth and J. Taborek of HTRI for consultation on the selection of test parameters, including fixes, the analysis and interpretation of test data, and the two-way communication with industry.

REFERENCES

1. Halle, H., and Wambsganss, M. W., "Tube Vibration in Industrial Size Test Heat Exchanger," ANL Technical Memorandum ANL-CT-80-18 (March 1980).

2. Wambsganss, M. W., and Halle, H., "Tube Vibration in Industrial Size Test Heat Exchanger (30° Triangular Layout - 6-Crosspass Configuration)," ANL Technical Memorandum ANL-CT-81-42 (October 1981).

3. Standards of Tubular Exchanger Manufacturers Association, Sixth Edition, New York, 1978.

4. Chen, S. S., and Jendrzejczyk, J. A., "Experiments on Fluid Elastic Instability in Tube Banks Subjected to Liquid Cross Flow," J. Sound Vib. 78(3), 355-381 (1981).

5. Connors, H. J., "Fluidelastic Vibration of Tube Arrays Excited by Nonuniform Cross Flow," PVP-41, Flow-Induced Vibrations of Power Plant Components, ASME, 1980.

6. Halle, H., Chenoweth, J. M., and Wambsganss, M. W., "DOE/ANL/HTRI Heat Exchanger Tube Vibration Data Bank," ANL Technical Memorandum ANL-CT-80-3 (February 1980).

7. Halle, H., Chenoweth, J. M., and Wambsganss, M. W., "DOE/ANL/HTRI Heat Exchanger Tube Vibration Data Bank - Addendum 1," ANL Technical Memorandum ANL-CT-80-3, Addendum 1 (January 1981).

8. Halle, H., Chenoweth, J. M., and Wambsganss, M. W., "DOE/ANL/HTRI Heat Exchanger Tube Vibration Data Bank - Addendum 2," ANL Technical Memorandum ANL-CT-80-3, Addendum 2 (November 1981).

9. Halle, H., Chenoweth, J. M., and Wambsganss, M. W., "DOE/ANL/HTRI Heat Exchanger Tube Vibration Data Bank - Addendum 3," ANL Technical Memorandum ANL-CT-80-3, Addendum 3 (January 1983).

10. Wambsganss, M. W., Yang, C. I., and Halle, H., "Fluidelastic Instability in Shell and Tube Heat Exchangers - A Framework for a Prediction Method," ANL Report ANL-83-8 (December 1982).

11. "HTRI ST-4 Computer Program for the Design or Rating of Shell-and Tube Heat Exchangers," Heat Transfer Research, Inc., Alhambra, CA, 1980.

12. Halle, H., Chenoweth, J. M., and Wambsganss, M. W., "Flow-Induced Tube Vibration Tests of Typical Industrial Heat Exchanger Configurations," ASME Paper 81-DET-37, 8th ASME Vibrations Conference, Hartford, CT (September 1981).

13. Chen, S. S., "The Instability Flow Velocity of Tube Arrays in Crossflow," Int. Conference on Flow Induced Vibrations in Fluid Engineering, Reading, England, Paper F2 (September 1982).

14. Chen, S. S., "Design Guide for Calculating the Instability Flow Velocity of Tube Arrays in Crossflow," ANL Technical Memorandum ANL-CT-81-40 (December 1981).

15. Chen, S. S., and Chung, H., "Design Guide for Calculating Hydrodynamic Mass, Part I: Circular Cylindrical Structures," ANL Technical Memorandum ANL-CT-76-45 (June 1976).

16. Connors, H. J., "Fluidelastic Vibration of Tube Arrays Excited by Nonuniform Cross Flow," Proc. of Flow-Indued Vibration in Heat Exchangers, ASME Winter Annual Meeting, New York, pp. 42-56, 1970.

17. Chen, S. S., "Instability Mechanisms and Stability Criteria of a Group of Circular Cylinders Subjected to Cross Flow. Part I: Theory," ASME Paper 81-DET-21; "Part II: Numerical Results and Discussions," ASME Paper 81-DET-22. Also in J. Vibration, Acoustics, Stress and Reliability in Design, Trans. ASME, Part I: 105, 51-58 (January 1983); Part II: future issue.

18. Pettigrew, M. J., and Campagna, A. O., "Heat Exchanger Tube Vibration: Comparison Between Operating Experiences and Vibration Analysis," Symposium on Practical Experience with Flow Induced Vibration, Karlsruhe, Germany, Sept. 3-6, 1979.

19. Crane Company, "Valves, Fittings," Catalog No. 60, Chicago, 1960.

20. Halle, H., and Wambsganss, M. W., "Shellside Waterflow Pressure Drop and Distribution in Industrial Size Test Heat Exchanger," ANL Report ANL-83-9 (January 1983).

APPENDIX

Summary of Sensory Observations: Cases 16-26

The tube bundle was backlighted and sensory (sight, sound, and feel) observations of tube bundle response were made as the flowrate was changed. In particular, tube motion was detected by sighting down the bores of the tubes, or by holding a finger against the tube ends where they come through the tubesheets. Rattling and impacting were audible and readily detected by ear. A case-by-case documentation of sensory observations made during testing is given below.

The flowrates are presented in gallons per minute (gpm), where 1 gal/min = 6.309×10^{-5} m^3/s.

Case 16

Full Bundle - 8 Crosspass - 10 in. Nozzles

Flowrate (gpm)	Observation
To 1200	No significant observation
1390	Quivering of shell periphery tubes S-21 and T-20
1600	Quivering of tubes S-21, T-20, U-19, also felt on central tubes of row B
1800	Same as 1600, some quiver also in a few row C tubes
2000	Same as 18, quiver in peripheral tubes S-21 (most), T-20, U-19 on bottom and S-3, T-4, and U-5 on top
2200	Tube S-21 active, moderate vibration tubes S-3, 4, 8, 9, 11, 15, and 16, T-4, 15, 16, 19 and 20, and U-19
2400	Impacting central tubes row S; also very active were tubes T-14, T-15, and U-14. After some delay more tubes S-16 through 21, T-16 through 20, U-15 through 17 and 19, and V-15 and 16 were found to be very active. Some row B tubes were buzzing at high frequency.
2600	Extended region of very active vibration if not impacting in far window, tubes S-7 to 21, T-10 to 20, U-10 to 19, V-15 and 16
2800	Very active/impacting region extends, including tube W-14

3000	Very active/impacting region extends throughout far window region except for tube U-5, 6, and 7 which are moderately vibrating and not impacting
3200	Same as 3000, U-5 also very active. High frequency vibration felt in row B and tubes C-15 and 16.
3400	Same as 3200 in far window. Also moderate vibration noted of some tubes in saddled rows R and F. Additionally, moderately vibrating in near window are tubes E-9, 12, and 13, D-11 to 14, and C-11. Quivering at high frequency are tubes A-10 and 11, and shell periphery tubes E-3, 4, 20, and 21.

Case 17

Full Bundle - 8 Crosspass - 14 in. Nozzles

Flowrate (gpm)	Observation
To 1400	No significant observation
1600	Slight quiver of tubes S-14, 17, 20 (strongest) and 21, T-20, E-4 and 5
1800	Quiver: tubes S-3, 10, 16, 19, 20, and 21; T-4, 20 and 21; E-4 and 5
2000	Moderate vibration of tubes S-16 through 21, T-19, and U-16 through 19 Quiver: tubes S-3, 10, 14, 15, T-4, 14, 15, 16; E-5, 9, 20 and 21
2200	Moderate vibration: tubes S-7 through 21, T-10 through 20, U-13 through 19, V-15 and 16, far window Quiver: tubes U-10, 11, and 12, V-11 through 14, W-11, 12, and 15. Also, in near window, tubes B-11, 12, and 13, D-20, E-3, 4, and 20, D-20
2400	All tubes in central and lower region of far window are active if not impacting. Impacting for certain are tubes S-10 through 14, T-10, 11, and 12; very active (if not impacting) are all tubes in their rows below S-8, T-8, U-9, V-9, and W-10. Moderate vibration of tubes S-3, 4, and 6, T-4, 6, and 7, as well as E-21, D-20, and C-16.

2600	Similar to above, with more tubes impacting. Moderate vibration of top tubes S-3, 4, and 5, T-4 through 7.
2780	Same as above, with more activity. Moderate vibration of near window tubes E-20 and 21, D-18, 19, and 20. Quiver of U-5 and 6.
3540	More active than above. Impacting initiates in row E next to baffle cut in near window. Very active, if not impacting, are E-10 through 19, D-10 through 14, C-12, and also U-5 and 6.

Case 18

No-tubes-in-window (NTIW) - 8 Crosspass - 14 in. Nozzles

Flowrate (gpm)	Observation
To 1200	No significant vibration
1600	Felt quiver of tube R-6
2000	Bottom tie bar seen vibrating through observation port on near side.
2400	Saddle row tubes R-5, 6, and 19 felt quivering.
2800	Quivering also felt in a few tubes of saddle row F
3200	More quivering in saddle rows R and F
3600	Many tubes in saddle rows R and F quivering; e.g., F-3 through 6, 13 through 19 and, R-3 through 6, R-17, 18, 19, and 21.
4000	Top tie bar on near window also vibrates. R-21 shuddering (but Q-22 is quiet); noticeable vibration of pairs R-10 and Q-10, F-12 and G-12. Back lighting across observation port permits observing motion of tubes in columns numbered 10 through 14.
4400	Tubes R-3, 17, and 21, and F-3 and 21 are shuddering. Tube bundle is noisy particularly on stationary end. Tie bar vibration observed in near window is estimated to be about 13 (0.25) and 6.5 mm (0.125 in.) on bottom and top, respectively.

4800	More active vibration. Tubes near top of bundles were vibrated loose to be moved to stationary side, including G-2 and 21, H-2, I-1 and 2, K-2, L-2, M-2, N-2, Q-2, P-2 and 6, also R-3, 9, 10, 11, 12, and 21. However, most lower tubes felt fairly inactive. Upon reaching this high flowrate another time, the top of the central baffle plate was observed to be pushed over by perhaps 5°, probably as a result of pressure differences. There was loud rattling/vibration noise, as if a tie bar was loose. Upon disassembly it was found that several tie bars had buckled.

Case 19

Full Bundle - 6 Crosspass - 14 in. Nozzles

Flowrate (gpm)	Observation
To 1200	No significant observations
1400	Quivering of tubes R-20 and 21, S-20 and 21
1600	Moderate vibration of tubes R-9 through 21, S-20 and 21, T-20, U-18 and 19. Quivering of tubes R-3, S-3, T-4 and 5, U-5 and 6. In one instant instability initiated but did not maintain itself. See case 19 discussion in text.
1700	Instability, with impacting quite certain, of tubes R-10 through 16, S-9 through 16; very active vibration with possible impacting of tubes R-7, 8, 9, 17, 18, and 19, S-8, 17 and 18, U-12 through 15; active vibration R-5, 6, 20 and 21, S-7, 19, 20, and 21, all of row T, U-9, 10, 11, 16, 17, and 18, V-8 and 9, and W-9. All other tubes in the far window appeared moderately active, so were, in addition, saddle row tubes Q-13, 14, and 15.
1810	Impacting, quite certain, of tubes R-7 through 18, S-7 through 16, T-7 through 15; very active vibration of tubes R-19 and 20; U-13 and 14; active vibration of tubes R-21, S-20 and 21, T-20; and moderate vibration of probably all others in window.
2000	Almost all near windows tubes active and many impacting. Moderate vibration only of tubes R-3, S-3, W-12, 13, and 14. Bottom tie bar in far window observed to vibrate.

2200	Most tubes in the internal region of the far window appeared to be impacting: tubes R-5 through 19, S-6 through 18, T-7 through 17, U-9 through 15. Tubes R-12 and R-15 were noticed to rotate.
2400	Tube S-10 observed to be rotating and leaking.
2800	Instability threshold in near window has been passed, instability region is in rows F and E, tubes 9 through 15 approximately. Lower shell periphery tubes F-21, and E-20 and 21, D-19 and 20, and E19 are more active than corresponding top tubes. After the flow had been shut down and the exchanger was tested again the next day, additional neighboring tubes also vibrated actively.
3000	Tubes in lower shell periphery region of tube rows R through V were probably impacting, too. Heard definite rumbling near G tap.

Case 20

Full Bundle - 6 Crosspasses - 10 in. Nozzles

Flowrate (gpm)	Observation
1200	No significant observations, slight quivering felt with finger in A and B rows.
1400	Quivering felt in tubes R-3 through 11, R-15 through 21, S-3, 4, 13, and 16; also rows A, B, and C tubes 10 through 14; low frequency quiver C-19.
1600	Same as 1400; most noticeable high frequency quiver in tube B-11, also tubes A-13 and 15, B-13, 15, and 16.
1700	Probable impact R-10 through 18, S-12 through 15, T-13 through 18 at time of observation (Note: subsequent data analysis showed that onset of instability was possible at 1650 but not necessarily sustained until 1730). Tube V-12 active, tubes R-3 through 7, S-3, and T-4 quivering.
1800	Central region, far window impacting, R-8 to 18, S-9 through 17, T-10 through 16 (probable).
1900	Impacting R-8 to 18, S-9 to 18, T-10 to 18. Active R-5 through 7, 19 through 21; S-6 through 8, 19 through 21, T-8, 9, 19, and 20; U-9 through 19; V-10 through 16; and W-11.

2000	Far window, most tubes impacting R-8 through 20, S-8 through 19, T-8 through 18; most others active. Near window active tubes near shell periphery B-8 (observed through port), C-5 and 19, D-4 and 20, E-3 and 21.
2400	Almost all tubes appear to be impacting except possibly R-3, S-3, T-4, U-5, and W-13 through 15. In near window, tubes in rows A, B, and C felt to vibrate at high frequency.
2800	Impacting of about 16 tubes in central region, rows E and F, tubes 8 through 15.
3200	Hard hitting vibrations of tube A-11.

Case 21

Passlane - Far Window Region

Flowrate (gpm)	Observation
To 1000	No significant observation
1200	Slight quivering felt with finger in tubes B-14 and 15, C-14 and 15.
1400	Additional and stronger quivering of tubes E-18 and 19. Quiet on far window side.
1600	Tubes B-15 and 16 quivering actively at high frequency, C-19 at low frequency. In far window, slight quivering of tubes R-8 through 14, T-20, and U-19.
1790	More quivering in row B than in row A, tube B-11 is much more active than A-11, quivering noticeably are tubes A-15, B-15 and 16, C-5 and 19, D-4 and 20. In far window there is quivering in central portion of rows R and S, also of top and bottom tubes of rows R through U near shell periphery. Tie bar vibration visible top and bottom in far window.
2000	Tubes R-7 through 17, S-7 through 16, and T-10 through 15 vibrate actively, if not impacting. (The No. 12 tubes are removed, of course). Row R through U tubes on the bottom of the far window near the shell periphery vibrate actively, the corresponding tubes on top vibrate moderately. Tubes W-9, 10 and 11 quiver, with U and W

	row tubes 13 through 15 almost quiet. In the near window tubes A-14 and 15 are felt strongly, C and D tubes 16, 17, and 18 are quivering. In the far window there is moderate tie bar vibration.
2200	Extended region of vibration compared to 2000. In far window tubes R-9 through 17, S-13 through 17, and T-12 and 13 are apparently impacting. Moderate vibration of tubes W-9, 10, 11, 14, and 15.
2400	Far window tubes R-7 through 17, S-8 through 17, T-9 through 16 are impacting. All remaining bottom row R, S, and T tubes as well as U-15 through 19, V-16 and 17 are very active. Moderate vibration of top tubes near shell periphery. Top tie bar vibrates strongly.
3000	Most far window tubes impact. In near window about 16 tubes in central region of rows E and F went into instability and impacting. Large tie bar vibrations occur, which don't diminish until flowrate returns to 1780 gal/min

Case 22

Passlane - Near and Far Window Regions

Flowrate (gpm)	Observation
To 1200	No significant observations
1400	Far window tubes R-3, S-3 and 4, and T-4 on shell periphery quiver. In near window, tubes quivering slightly are row A, row B and C tubes 8 through 15 in central region; and C-5, 18, and 19, D-4, 5, 18, 19, and 20, and E-21 near shell periphery. Tube B-16 quivers moderately.
1600	Tubes R-4 through 11, and S-11 quiver, but R-13 is quiet. In the near window many tubes in rows A, B, and C quiver, also top and bottom tubes on shell periphery and row A through F No. 11 and 13 tubes next to passlane.
1800	In far window as 1600, in addition quiver of top and bottom shell periphery tubes. In near window most row A through D tubes, also along passlanes the A through F No. 10, 11, 13, and 14 tubes. High frequency buzz felt on tubes C-19, D-19 and 20. Quiver seen on tie bars.

2000	Similar to 1800. Quivering in all of row R. Tie bar vibrating slightly.
2200	Large vibration amplitudes, if not impacting, of tubes R-11, 13 through 17; S-11, 13 through 17, T-11, 13, and 14. Actively vibrating are the remaining tubes of row R, tubes S-9, 10, 20, and 21, T-9, 10, and 20, U-9 and 10. Moderately vibrating are tubes near shell periphery rows R through U, also V-8 and 9, and W-9. Central tubes in saddled row Q are vibrating slightly. In near window, high frequency buzz felt in tubes in rows A through D.
2400	Except for shell periphery tubes row R through U which were vibrating actively, all row R and S tubes and all row T tubes above the passlane and T-13 had large vibrations if not impacting. Most other far window tubes were seen vibrating, but row W tubes were relatively quiet. Tie bars seen vibrating in window, more on top.
2800	Tube S-21 vibrates with large amplitudes in the 45° direction. Large tie bar vibration seen in observation port.
3200	Most tubes in far window vibrate a lot. This can readily be seen in observation port.

Case 23

NTIW - 6 Crosspasses - 10 in. Nozzles

Flowrate (gpm)	Observation
To 800	No significant obsrvations
1000	Tie bars are observed to vibrate slightly in "far window" observation port
1200	Tie bar vibration is small, but lower more active
1400	Same as 1200, tie bar vibration is shuddering (i.e., beating irregularly)
1600	Small increase of tie bar vibration, now upper tie bar is more active. All row G and H tubes quiver, with No. 8 and 9 tubes most noticeable.
2000	All row G and H tubes from the top through No. 13 vibrate slightly, with H-8 and 9 most. Row G and H tubes No. 14

	and below were only quivering, except G-18 and Q-2 that vibrated slightly. Tie bar vibration peak to peak amplitude is about 2.5 mm (0.1 in.) and 1.5 mm (0.06 in.) on top and bottom, respectively. Distinct ticking heard on end of tie bolt V-7 only.
2400	More of slight vibration activity in row H than G, tubes H-8 and 9, G-11 and 12 are most active. All four tie bolts B and V, 7 and 17, gave audible (stethoscope) indication of being struck, apparently by tie bars.
2650	Noticeable clicking started due to apparently large tie bar vibration.
2800	General noise increase. Tie bar observed vibrating with approximately 5 mm (0.2 in.) peak-to-peak amplitude.
3200	Tube Q-2 and all row G and H tubes, except H-21 and 22, vibrating actively. The tie bars can be heard striking shell.
3600	Similar to 3200. Strong high frequency vibration of G-11 and 12, H-2 through 14 (more than row G), Q-2 and 3. Observed strong vertical movement to the extent of the baffle hole in the saddled Q row through porthole.

Case 24

FIVER

Flowrate (gpm)	Observation
To 800	No significant observations
1000	Felt slight quiver with finger on a few tubes in central region rows A through D
1200	Same as 1000, also slight quiver in C-7 and 18, D-15 and T-4.
1600	Quivering of tubes rows A and B, 9 through 15, C-18 and 19, D-5 through 16, E-3, T-4 and 14, U-5 and 6, V-8 and 16.
1800	About same as 1600, quivering also felt in tubes C-19, D-20, S-3 and 21. Noticeable high frequency buzz felt in tubes A-12 and 13, B-12 and 13.

2000	Far window shell periphery tubes S-3 and 21, T-4, and U-5 vibrate slightly. Tubes T-13 and 14, and U-13 quiver. All tubes in near window can be felt to vibrate.
2200	Similar to 2000, additional tubes in far window shell periphery vibrating slightly. Tube Q-2 can be felt. Buzzing is strong in row A, less in tubes B-9 through 15, still less in tubes C-9 through 15.
2400	Additional slight vibration of tubes S-3 and 21 and V-21. Tube rows A through C, top through 13 are buzzing. Slight vibration of lower tie bar in far window.
2600	Moderate vibration of tubes T-4, 5, and 6 U-5, 6, and 7, and V-8. All near window tubes in rows A through D are buzzing. Slight shuddering of lower tie bar about 1.5 mm (0.06 in.) peak-to-peak.
2800	About as 2600. Strong buzz in rows A and B, Nos. 11, 12, and 13 tubes.
3000	Tubes T-9 through 15, and U-10 through 14 were impacting, neighboring tubes vibrated very actively. Tubes W-9 and 10 were active. Strong buzz in tubes A-9 through 13, and B-8 through 16. Tie bars vibrate about 2.5 mm (0.1 in.) peak-to-peak.

Case 25

Full Bundle - Finned Tubes

Flowrate (gpm)	Observation
800, 1000	Slight quiver felt in some near window tubes
1200	Tubes C-11, 13, and 19 quiver slightly more than others.
1400	In far window no vibration noticeable except slight quiver in central tubes. In near window there is gentle buzzing in central region but also of tubes A-9, B-8, C-18 and 19, and D-20.
1600	As 1400, also slight vibration of T-20 and 21 and some low frequency activity in central far window.
1800	Increase of vibration in central region of far window. Looked like it was about to go unstable, but did not do

	so. Slight buzz felt on almost all tubes in near window, specifically C-18 and 19, D-4, and E-3. More buzz on rows C and B than on A.
2000	As 1800, tubes R-9 through 13, S-9 through 12, and T-9 through 12 are active.
2330	Initial impacting of tubes R-9 through 14, S-9 through 12, T-9 through 12, and U-12.
2440	Impacting region in central region of far window extends more towards top than bottom.
2800	Impacting are far window tubes R-8 through 16, S-8 through 17, T-8 through 13, U-11 and 12. Near window tubes E-12 through 15, F-12, 13, and 14 are active.
3200	Instability has also initiated in near window, with apparent impacting (in a region biased toward the top of the bundle) of tubes D-10, 11, and 12, E-9 through 13, and F-7 through 15.

Case 26

NTIW - Finned Tubes

Flowrate (gpm)	Observations
To 1200	No significant vibration
1600	Very slight quivering of tube Q-13. Far window tie bars seen vibrating with about 1.5 mm (0.06 in.) peak-to-peak amplitude.
1800	As 1600, slight quivering of some row G tubes (most on G-22) felt.
2000	About same as for 1800, most quivering of G row were tubes G-17 and 22. Far window tie bar amplitudes about 3 mm (0.12 in.) and 1.5 mm (0.06 in.) on top and bottom, respectively, as seen through observation port.
2080	It appears that that far window, top tie bar started to strike shell near stationary end.
2400	Most row G tubes felt but not sen to vibrate. Top tie bar vibrating strongly.

2800	Quiver seen on tubes Q-13, and 22, and H-12. Buzzing felt on many row G, H, and I tubes, most in central region. Tie bar peak-to-peak amplitudes 6 mm (0.25 in.) and 3 mm (0.12 in.) on top and bottom respectively.
3200	Tubes Q-13, 21, and 22 quiver, otherwise far window rgion fairly quiet. In central region of near window buzz over a large area up to center of row K. Also strong buzz of lower shell periphery tubes G-20, 21, and 22, and H-21 and 22.
3600	About same as 3200. Quiver noticed also in Q-2. Rate of tie bar vibration hitting increased with flow. Peak-to-peak amplitudes about 9.5 mm (0.38 in.) and 4.8 mm (0.19 in.) at top and bottom, respectively.
4140	Strong buzz felt on tubes Q-2, 3, 4, 11, 12, 13, 20, 21 and 22. Near window buzz about as before extending to row L in central region. Wild vibration and beating of tie bars.
4650	Strong buzz tubes Q-9 through 17, in rows Gand H tube 11, 12, 13, 21, and 22. Moderate buzz in rows O and P tubes 7 through 19.
5270	Almost all tubes indicate high frequency buzzing, strong for row G and H tubes 2, 3, 9 through 17, 21 and 22;row I-1, 2, 3, 10 through 15, 22 and 23; J-1, 2, 3, 11 through 15, and 22; rows O and P tubes 10 through 15, and Q-9 through 17.